Aus der Klinik für Neurologie

(Prof. Dr. med. M. Bähr)

der Medizinischen Fakultät der Universität Göttingen

Hypoxic Microglial Extracellular Vesicles Abrogate Poststroke AQP4 Depolarization, Astrogliosis and Neuroinflammation

INAUGURAL-DISSERTATION

zur Erlangung des Doktorgrades

der Medizinischen Fakultät der

Georg-August-Universität zu Göttingen

vorgelegt von

Wenqiang Xin

aus

Fuzhou, Jiangxi, China

Göttingen 2023

Dekan: Prof. Dr. med. W. Brück

Betreuungsausschuss

Betreuer/in: Prof. Dr. med. T. R. Döppner, M.Sc.

Ko-Betreuer/in: Prof. Dr. med. G. Wulf

Prüfungskommission

Referent/in: Prof. Dr. med. T. R. Döppner, M.Sc.

Ko-Referent/in:

Drittreferent/in:

Datum der mündlichen Prüfung:

Hiermit erkläre ich, die Dissertation mit dem Titel "Hypoxic Microglial Extracellular Vesicles Abrogate Poststroke AQP4 Depolarization, Astrogliosis and Neuroinflammation" eigenständig angefertigt und keine anderen als die von mir angegebenen Quellen und Hilfsmittel verwendet zu haben.

Göttingen, den 18/04/2023 (Unterschrift)

TABLE OF CONTENTS

LIST OF FIGURES

LIST OF FIGURES

LIST OF TABLES

ABBREVIATIONS

AT1R	angiotensin II type 1 receptor
AMP	adenosine monophosphate
ATP	adenosine-triphosphate
AS	astrocytes
AMPK	AMP-activated protein kinase
AQP	aquaporins
ANOVA	analysis of variance
BCA	bicinchoninic acid
CBF	cerebral blood flow
CS	complete stroke
cGMP	cyclic guanosine monophosphate
CNS	central nervous system
CH25H	cholesterol-25-hydroxylase
DS	donkey serum
EV	extracellular vesicle
HDL	high-density lipoprotein
HPY	hypoxanthine
iNOS	inducible nitric oxide synthase
IL	interleukin
INF-y	interferon-y
ICH	intracerebral hemorrhage
LDL	low-density lipoprotein
LPS	lipopolysaccharide
MV	microvesicle
MVB	multivesicular bodies
MTT	3-(4,5 -dimethylthiazol-2-yl)-2,5-diphenyltetrazolium bromide
MCAO	middle cerebral artery occlusion
NTA	nano-track analysis
NS	not statistically significant
NO	nitrogen monoxide
OGD	oxygen-glucose deprivation
PDL	poly-D-lysine
PEG	polyethylene glycol

ABBREVIATIONS

PFA	paraformaldehyde
PBST	phosphate-buffered saline solution with Tween detergent
ROI	region of interest
RIND	reversible neurological dysfunction
RIPA	radioimmunoprecipitation assay
SDS-PAGE	SDS-polyacrylamide gel electrophoresis
SIE	progressive stroke
SAH	subarachnoid hemorrhage
TBS	tris buffered saline
TLR	Toll-like receptor
TEM	transmission electron microscopy
TSG101	tumor susceptibility gene 101
TNF-α	tumor necrosis factor-α
TGF-13	transforming growth factor-13
TIA	transient ischemic attack
XO	xanthine oxidase
Xan	xanthine

ABSTRACT

Reactive astrogliosis, aquaporin 4 (AQP4) depolarization and neuroinflammation occurring and lasting for a long time in the periinfarct region are associated with poststroke brain injury. Our previous work has revealed that extracellular vesicles (EVs) from hypoxic microglia are implicated in protecting against stroke-induced brain damage. Uncertainty persists regarding how poststroke immunological regulation and AQP4 depolarization are affected by hypoxia-induced microglial EVs. Mice were administered with hypoxic microglial EVs via tail vein injections. Cerebral perfusion, edema of the brain, and neurological function were detected after induction of ischemia in the MCAO mouse model. AQP4 polarization, astrogliosis, and neuroinflammation were evaluated in the brain cortex after ischemia. Employing primary astrocytes and microglia subjected to oxygen-glucose deprivation (OGD) *in vitro*, we evaluated the role of EVs in microglial polarization and astrocytic inflammation and AQP4 expression. Furthermore, a notion is given to the role of AQP4 levels in astrocyte–microglia inflammation communication via establishing a co-culture system between primary astrocytes and microglia. *In vivo*, EVs from hypoxic microglia promote postischemic cerebral perfusion and motor coordination impairment and diminished postischemic brain edema. Such EVs in the meantime cut peri-infarct AQP4 depolarization, astrogliosis, and inflammation. *In vitro*, a hypoxic condition promoted cortical M2 microglial polarization, and an increased concentration of such EVs in hypoxic microglia was related to a higher release of the M2 microglial polarization biomarkers and a lower release of the M1 microglial polarization biomarkers. Furthermore, EVs attenuated the upregulation of AQP4 clustering and pro-inflammatory molecules in the cortical astrocytes challenged by hypoxia. However, an alteration of the AQP4 expression in astrocytes was not involved in modulating astrocyte-to-microglia inflammation communication. Therefore, the data illustrate, for the first time, that hypoxic microglia can participate in protecting against stroke-induced brain damage by diminishing poststroke neuroinflammation, astrogliosis and AQP4 depolarization via releasing EVs, indicating that this investigation may represent a novel perspective for stroke treatment.

1. Introduction

1.1. Ischemic Stroke

Currently, stroke is one of the most difficult situations doctors see in hospital emergency rooms, which needs to be instantaneously safeguarded by neurological integrity (Gil-Garcia et al. 2022). By 2030, it is predicted that there will be 7.8 million deaths related to stroke and 23 million stroke patients (Malik et al. 2021). Stroke is described as "quickly evolving clinical symptoms of focal disruption of brain function, lasting more than 24 h or causing patient death with no clear cause beyond that of vascular origin" by the World Health Organization (Gil-Garcia et al. 2022). A stroke, also referred to as a cerebrovascular accident, is a condition in which brain tissue is damaged by the abrupt rupture of a blood vessel in the brain or by obstruction of a blood vessel that prevents blood from flowing to the brain. Ischemic stroke and hemorrhagic stroke are two types of strokes (Turnbull et al. 2019). Hemorrhagic strokes, which account for 15% of all strokes and 40% of stroke-related death, include intracerebral hemorrhage (ICH) and aneurysm rupture-induced subarachnoid hemorrhage (SAH) (Yang et al. 2017). The most typical form of hemorrhagic stroke is ICH. Even though ICH and SAH may now be swiftly discovered and treated, over 50% of stroke patients still require one year of care after the original ictus and have memory, speech, and daily activity deficits (Hackett and Anderson 2000).

According to a recent report by the American Heart Association, ischemic strokes occur more frequently than hemorrhagic strokes and account for more than 85% of all stroke cases (Benjamin et al. 2018). The phrase "ischemic stroke" refers to the necrosis of neural tissue brought on by thrombosis-induced narrowing or obstruction of the brain's feeding arteries (the carotid and vertebral arteries) and inadequate blood flow to the brain. Four different forms of cerebral ischemia exist: Reversible neurological dysfunction (RIND); progressive stroke (SIE); complete stroke (CS); and transient ischemic attack (TIA). TIA shows no cerebral infarction, while RIND, SIE, and CS show different degrees of cerebral infarction with corresponding clinical manifestations of neurological loss. Importantly, it is estimated that three-quarters of cases with ischemic stroke drop out of the labor force, and two-fifths of these participants yield severe disability (Uyeki et al. 2016). Annually, 51.9 million years are lost to ischemic stroke-related disability, showing an enormous economic and social impact of ischemic stroke (Wafa et al. 2020).

1.2. Etiology

An embolus in arteries supplying the brain is the most frequent cause of an ischemic stroke. Atherosclerosis is the primary cause of internal carotid artery or vertebral artery stenosis, and an atheromatous plaque's vulnerability is what gives it the most pathogenic relevance in ischemic stroke (Rink and Khanna 2011). A major lipid core with more than 40% of foam cells packed with low-density lipoprotein (LDL) and a thin fibrous top with fewer smooth muscle cells make up vulnerable plaques (Hellings et al. 2007). Besides, an abundant infiltration of inflammatory macrophages is another major biomarker for the vulnerability of plaques (Rink and Khanna 2011). Apart from atherosclerotic plaque effects, individuals with atrial fibrillation and coronary heart disease are more likely to develop mural thrombosis in their heart valves, which block the cerebral artery and lead to an ischemic stroke after shedding emboli (Rink and Khanna 2011). Other common risk factors include hypertension and hyperlipidemia. The principal risk factor for stroke is hypertension, particularly an unusual rise in blood pressure in the morning. An earlier study discovered that the strongest independent predictor of stroke occurrences was morning hypertension (Kario et al. 2006). The risk of an ischemic stroke jumped by 44% for every 10 mmHg rise in the morning, and it was four times higher in the morning than at other times of the day. The angiotensin II type 1 receptor (AT1R) polymorphism and increased vascular oxidative stress were uncovered to be vital contributors to yield sympathetic hypertension and vascular disease (Mettimano et al. 2002). It is well-recognized that hyperlipoidemia raises the risk of ischemic stroke and reduced cerebral perfusion. The effects of statins (an inhibitor for hyperlipoidemia) in patients with coronary artery disease have demonstrated their contribution to ischemic stroke prevention because statins have a strong inverse correlation with atherosclerosis via regulating plasma high-density lipoprotein (HDL) levels (White et al. 2000). Additionally, many pathological and behavioral conditions have been demonstrated to yield a higher risk of ischemic stroke (Barthels and Das 2020; Boehme et al. 2017). These factors include but are not limited to diet, smoking habits, and diabetes (Barthels and Das 2020). Since these risk factors have an important impact on keeping the cardiovascular system in good condition, they are the useful way to predict the likelihood of having an ischemic stroke. However, a lot of these risk factors that contribute to the development of ischemic stroke are controllable; as a result, it is essential to lower these risk factors and engage in physical activity in order to lower the risk of ischemic stroke in higher risk groups.

1.3. Pathogenesis

1.3.1 Cell death

Despite the emergence of calcium overload, toxic free oxygen radicals and excitotoxicity, which laid a foundation for explaining the pathophysiology of ischemic stroke, some drugs for ischemic strokes, such as calcium channel blockers, free radical scavengers, and excitatory amino group antagonists, have also emerged, but so far there are no ideal therapeutic drugs (Trouillas and von Kummer 2006). Therefore, it is still a difficult task to figure out the ischemic stroke pathophysiology. Neuronal cell death, including apoptosis and necrosis, plays an essential role in the clinical symptoms that appeared in cases with ischemic stroke. While apoptosis predominates in the cells in the penumbra, necrosis manifests in the ischemic core. Apoptosis refers to programmed cell death, whereas cell necrosis is a passive death process (Karch and Molkentin 2015; Radak et al. 2017). The morphological and biochemical features of apoptosis include cell shrinkage, nuclear chromatin concentration, and DNA fragmentation, while cell membrane structure and organelles remain intact (Radak et al. 2017).

1.3.2 Cell autophagy

Furthermore, another type of cell death known as autophagy is a wholly natural, regulated process that eliminates and recycles long-lived, misfolded proteins, insoluble proteins, and damaged organelles for the balance of energy and function homeostasis of cells (Shi Q et al. 2021). Under ischemic stroke conditions, insufficient oxygen and glucose results in a higher ratio of adenosine monophosphate (AMP)/adenosine-triphosphate (ATP), which meantime will promote the AMP-activated protein kinase (AMPK) pathway to activate the autophagy process (Shi et al. 2021). A great amount of evidence indicates that autophagy has a double-edged sword effect during the pathogenesis of ischemic stroke (Shi Q et al. 2021). Multiple studies have confirmed that autophagy may be a therapeutic target in ischemic stroke (Wei et al. 2022). Other research has linked autophagy to the promotion of cell death (Wei W et al. 2022).

1.3.3 Free radicals and nitrogen monoxide (NO)

During cerebral ischemia and reperfusion, when intracellular Ca^{2+} concentration increases, intracellular Ca^{2+}-dependent proteolytic enzymes are activated, and xanthine dehydrogenase is converted to xanthine oxidase (XO) (MacDonald et al. 2006; Pignataro et al. 2014). ATP-degrading metabolites such as hypoxanthine (HPY) and xanthine (Xan) increase. XO causes a significant amount of harmful oxygen free radicals to be created. The epoxidase pathway

metabolizes arachidonic acid to target DNA and membrane structure, causing damage to cellular function and structure. In addition, oxygen free radicals produced by the NO pathway also play important roles as follows (Samdani et al. 1997; Wierońska et al. 2021): (I) Effect on cerebral circulation: NO is a strong vasodilator, inhibiting platelet aggregation and leukocyte adhesion. Under physiological conditions, cyclic guanosine monophosphate (cGMP), which is produced by the endothelium, neurons, and glial cells, acts on smooth muscle cells to dilate cerebral blood vessels and increase cerebral blood flow (CBF); (II) Effects on brain injury: NO has both beneficial and harmful effects. On the positive side, in addition to improving CBF, after a few hours of cerebral ischemia, NO no longer protects the cerebral blood flow and becomes harmful.

1.3.4 Neuroinflammation

An important factor in the overall pathophysiology of ischemic stroke is neuroinflammation. The inflammatory response has two opposing effects, first causing ischemic brain damage, and second promoting tissue repair (Fann et al. 2013). Numerous pro-inflammatory cytokines, including tumor necrosis factor-α (TNF-α), NO from inducible nitric oxide synthase (iNOS), interleukin 1 (IL-1), IL-6, IL-12, and IL-18 are released to start the inflammatory response (Fann et al. 2013; Jin et al. 2013). The release of these cytokines by neurons, astrocytes, microglia, and endothelial cells leads to the death of neurons and glial cells. These cytokines can activate a variety of adhesion molecules on leukocytes, endothelial cells, and platelets, including intercellular adhesion molecule-1, vascular adhesion molecules, selectins, and integrins (DeGraba 1998; Fann et al. 2013).

1.4. Treatment

Ischemic stroke is an emergency and rescue disease. Clinically, it is considered that the best time window for its treatment is up to 6 h after the onset. The purpose of various treatment methods is to establish collateral circulation for the brain, restore the damaged brain tissue's blood and oxygen supply, and rescue the damaged neurons as much as possible.

1.4.1 Thrombolytic therapy

Thrombolytic therapy is commonly used in treating ischemic stroke and is considered to be the most effective drug therapy for stroke. Thrombolytic therapy refers to the administration of thrombolytic drugs to patients (Mendelson and Prabhakaran 2021; Taussky et al. 2011). The function of these thrombolytic drugs is to promote and accelerate the dissolution of thrombosis in the blood, accelerate blood circulation, and restore blood circulation (Taussky

et al. 2011). Thrombolytic therapy can be divided into intravenous and arterial thrombolytic therapy (Mendelson and Prabhakaran 2021). Thrombolytic agents widely used in intravenous thrombolytic therapy mainly include streptokinase, urokinase, and tissue plasmin activator (Ospel et al. 2020). Urokinase is mainly used in ischemic stroke patients with onset within 6 h (Suardika and Astawa Pemayun 2018). Streptokinase is applied to patients within 3 to 4 h after the onset of stroke, but it has been found to increase the risk of vascular bleeding. Tissue plasminogen activator, a second-generation thrombolytic drug, has a significant therapeutic effect on stroke patients within 3 h of onset (Klegerman 2017; Prabhakaran et al. 2015). Arterial thrombolysis is often utilized to treat patients with ischemic stroke in an emergency. Arterial thrombolysis can allow rapid removal of large proximal thrombi. The benefits of arterial thrombolysis in patients with ischemic stroke were demonstrated by the outcomes of multiple prior prospective trials, and as a result, it became a routine form of treatment (Campbell et al. 2015; Goyal et al. 2015). Meanwhile, thrombolytic therapy can also lead to complications such as intracranial hemorrhage and reperfusion injury. Therefore, it is necessary to evaluate the risk, weigh the pros and cons, and strictly control the dose, type and time of thrombolytic agents to reduce complications.

1.4.2 Surgical treatment

There is still some controversy about the necessity of surgical treatment of ischemic stroke patients, however, some scholars agree that early surgical treatment has a beneficial impact on enhancing stroke patients' prognosis (Lilja-Cyron et al. 2016). It is generally accepted that surgical treatment should be used for ischemic stroke patients with a living ability of grade II-IV, and surgical treatment is better than conservative treatment for such patients (Nagaraja et al. 2018). Consciousness is one of the important indexes judging the adoption of surgery. The patients admitted to the hospital with consciousness gradually blurred indicate that the patient may have an enlarged infarct area, increased intracranial pressure, and brain edema, and surgical treatment should be performed as soon as possible. Once bilateral pupil dilation occurs, the best time for surgical treatment may be missed (Unterberg and Juettler 2007). To lower intracranial pressure and restore brain tissue in eligible patients, surgery should be performed as early as possible (Unterberg and Juettler 2007).

1.4.3 Other treatments

Other treatments include anti-platelet aggregation, anticoagulants and neuroprotection therapy. Patients with ischemic stroke are mostly in a hypercoagulable state owing to the platelet aggregation, hence anti-platelet aggregation drugs may be beneficial for them (Diener 2000). Anticoagulant therapy may have a good effect on the prevention of stroke and the

expansion of thrombosis (Kapil et al. 2017). Neuroprotection therapy mainly has the efficacy of repairing damaged neurons (Zhao et al. 2022). Currently, the primary neuroprotective agents include calcium antagonists, glutamate antagonists, cell membrane stabilizers, γ-aminobutyric acid receptor agonists, glutamate release inhibitors, and free radical scavengers (Mosconi and Paciaroni 2022).

1.5. Astrogliosis and AQP4 depolarization in ischemic stroke

The most abundant form of glial cells in the human brain are astrocytes (Fischer et al. 2014). Astrocytes are involved in a variety of functions in the central nervous system (CNS), including scaffold support, blood-brain barrier creation and regulation, neuronal growth and damage healing, neuroimmune regulation and neurotransmitter metabolism (Linnerbauer and Rothhammer 2020). However, astrocytes were also shown to have some negative effects after ischemic stroke. Astrocytes are the key regulators of inflammatory response in the CNS (Colombo and Farina 2016). Following a stroke, the activation of astrocytes causes the production of several inflammatory mediators, including TNF-α, IL-1β, IL-6 and cell adhesion molecules (Stoll et al. 1998), and nitric oxide and other neurotoxic mediators are produced as a direct or indirect result of these inflammatory mediators (Liddelow and Barres 2017). The blood-brain barrier permeability is augmented, and an inflammatory cascade is triggered, which further aggravates the ischemic stroke injury (Nayak et al. 2012). More importantly, astrocyte activation, proliferation, and migration lead to the formation of glial scar formation (Huang et al. 2014; Koyama 2014). The dense glial scar makes it difficult for the regenerating axons to cross, by that forming a physical barrier to neuronal regeneration (Choudhury and Ding 2016; Huang et al. 2014). The extracellular matrix components chondroitin sulfate proteoglycans and tendinin, which block axonal growth, generate chemical barriers, and prevent neuron regeneration following damage, can be secreted by these activated astrocytes (Pekny et al. 2014). Therefore, reducing reactive astrogliosis and astrocyte hyperplasia appears beneficial after an ischemic stroke.

Aquaporins (AQPs), a class of transmembrane proteins, are related to water regulation in the brain (Dasdelen et al. 2020; Kruse et al. 2006). Currently, 13 different AQPs (AQP0-12) have been found in mammals, among which AQP4 is the most widely distributed in brain tissue (Badaut et al. 2014). AQP4 is mostly found in astrocytes, ependymal epithelial cells, choroid plexus epithelial cells, and vascular endothelial cells (Assentoft et al. 2015). It is particularly abundant in astrocytic endfeet, which are located next to capillaries, arachnoid membranes, and leptomeninges (Ikeshima-Kataoka 2016). The astrocytic endfeet surround the blood

arteries to form the so-called 'neurovascular unit' as part of the blood-brain-barrier (Ballabh et al. 2004). Here, AQP4 is primarily expressed in a polarized distribution (Ren et al. 2013). AQP4 facilitates the rapid entrance or outflow of water into or out of the brain. Under pathological conditions, AQP4 can lose its polarity, manifested as scattered distribution on the plasma membrane of astrocytes, a phenomenon called "depolarization" (Ren et al. 2013). This leads to the development of edema and furthermore impairs the removal of interstitial solutes from the brain via AQP4-mediated water transport. In the peri-infarct region, loss of perivascular AQP4 polarization after ischemic stroke manifests and persists for a considerable amount of time (Filchenko et al. 2020; Ji et al. 2021; Mogoanta et al. 2014). Inhibiting the depolarization of AQP4 with the inhibitor TGN-020 after an ischemic stroke reduced brain edema, attenuated peri-infarct astrogliosis, and attenuated AQP4 depolarization (Sun et al. 2022). Consequently, restoring AQP4 polarization in the peri-infarct region may be a useful therapeutic approach after stroke to improve the restoration of neurological function.

1.6 Microglia-associated inflammation in ischemic stroke

As already mentioned, the inflammatory response plays a crucial part in neurocyte survival and the restoration of neurological function following an ischemic stroke. Microglia are a type of glial cell that make up 10 to 15% of all glial cells in the CNS (Sieweke und Allen 2013). The embryonic myeloid progenitors in the yolk sac give rise to microglia, which move through the circulation to the CNS. Microglia, a subclass of CNS macrophages, represent the CNS quickest and most crucial immunological barrier (Filiano et al. 2015). Under resting conditions, microglia are capable of phagocytosis and remain quiescent, playing an immune role in monitoring the special environment in which nerve cells grow. When they detect pathogen invasion or tissue injury, they are rapidly activated to initiate an inflammatory response (Xiong et al. 2016). What is more, microglia are particularly sensitive to ischemic stroke. In response to ischemic stimulation, resting microglia would be immediately activated, initiating an inflammatory cascade (Michels et al. 2017). Various inflammatory cytokines and neurotoxic mediators are secreted by them (Xu et al. 2020). On the contrary, microglia can also release anti-inflammatory substances to safeguard neuronal function (Ma et al. 2017).

There are two activation types of microglia: M1 and M2. While M1 microglia can present antigens and take part in the proinflammatory tissue response, M2 microglia can eliminate necrotic tissue, promote tissue repair, and maintain homeostasis by releasing a variety of anti-

inflammatory compounds (Qin et al. 2019). M1 microglia is the classically activated type, mainly expressing CD80, CD86, major histocompatibility complex, and can secrete IL-1β, IL-6, iNOS, interferon-y (INF-y), and TNF-α (Lan et al. 2017; Xin et al. 2021). The M2 type is a substitution-activated type, which mainly expresses surface antigens such as YM1 and CD206, and secretes IL-10, IL-4, IL-3, transforming growth factor (TGF)-13 and insulin-like growth factor-1 (IGF 1) as anti-inflammatory factors (Xin et al. 2021). M2-type microglia can also secrete many neurotrophic factors, which can prevent brain damage in cerebral stroke (Wang et al. 2018). Three different M2 types of microglia can be distinguished: M2a, M2b, and M2c. The M2a type is primarily involved in cell regeneration, whereas the other two varieties are mostly involved in phagocytosis and the clearance of necrotic tissue (Chhor et al. 2013; Xin et al. 2021). Promoting the M2 phenotype and inhibiting the M1 phenotype, or phenotypic manipulation between the M1 and M2 types could thus be advantageous to improve poststroke recovery by controlling inflammatory variables.

1.7 Extracellular vesicles and cell-cell communication

Through direct cell-cell contact or signalling molecules, multicellular organisms can accomplish their regular physiological processes. In the past two decades, the way of intercellular communication has been further elucidated, bringing extracellular vesicles (EVs) more into the focus. Despite the fact that the release of apoptotic bodies during apoptosis has long been reported, more recently, the release of vesicles from healthy cell membranes was discovered. EVs, nano-sized membrane vesicles, carry RNA, DNA, proteins, lipids, and other molecules (Li et al. 2022). They can be found in a variety of body fluids, including amniotic fluid, cerebrospinal fluid, breast milk, serum, plasma, saliva, and urine (Hermann et al. 2022). Currently, three main subsets of EVs have been found **(Figure 1)**, including exosomes, microvesicles (MVs), and apoptotic bodies (Hermann et al. 2022). Exosomes have a mass of 1.13-1.19 g/ml and a length of 30-150 nm (Yang et al. 2020). Exosome release includes several steps: First, the cell membrane is invaginated to yield a primary endosomal membrane and further forms multivesicular bodies (MVBs). MVBs are important in protein transport and sorting in eukaryotic cells (Gurung et al. 2021). When MVBs fuse with the cell membrane, the lumen-like vesicles are depressed, and granular vesicles with a length of 30-150 nm are formed by internal budding and released into the extracellular environment, namely exosomes (Van Niel et al. 2018). MVs are larger vesicles that are formed by the cytoplasmic membrane directly projecting out of the cell in a budding manner, with a diameter of 200-1,000 nm (Thietart and Rautou 2020). Finally, dying cells secrete apoptotic

bodies, the biggest EVs of all with a diameter of 1,000–5,000 nm in length (Battistelli and Falcieri 2020; Doyle and Wang 2019). Yet, due to discrepant sizes brought on by various measuring procedures, the vesicle size that was once thought to be a crucial feature to discriminate between distinct subtypes is no longer regarded as useful. In the meanwhile, rather than size, the function of EVs is mostly determined by their cargo.

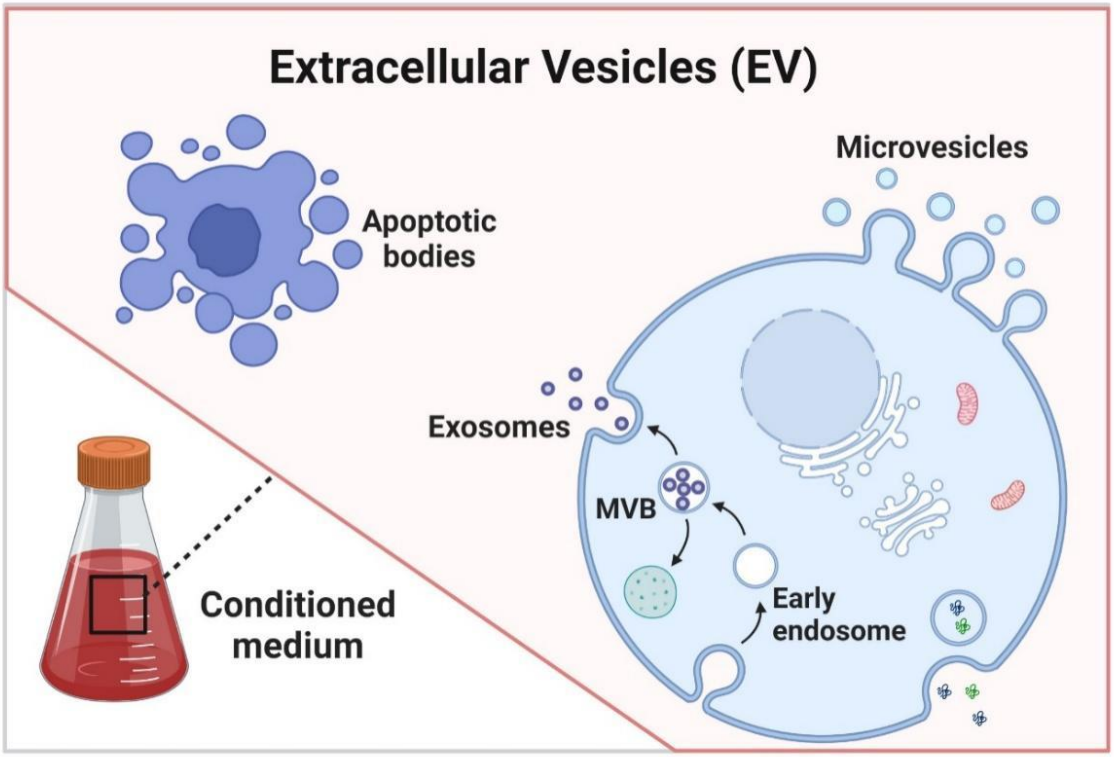

Figure 1: Characterization of extracellular vesicles (EVs).EVs have three main subsets, including exosomes, microvesicles, and apoptotic bodies.

After release, EVs can be isolated by adopting ultracentrifugation with a 100,000-200,000 ×g. Given that a great number of non-vesicular cargo including RNA, protein, and DNA exists in the extracellular setting, it is required to characterize the extracted EVs using a variety of methods (transmission electron microscopy (TEM), nano-track analysis (NTA), western blot). Single vesicles with irregularly shaped membranes could be found using TEM (Zhang et al. 2021b). NTA from enriched EVs can be used to depict vesicle concentration and size distribution patterns. The western blot can be conducted to recognize protein markers of EVs. EVs can be identified by a number of proteins, including CD63, CD9, CD81, Alix, tumor susceptibility gene 101 (TSG101), and many others (Jeppesen et al. 2019). Numerous studies have shown that EVs are essential for the prevention and treatment of ischemic stroke (Zheng et al. 2021a) and that EVs produced from microglia, mesenchymal stem cells,

and astrocytes, have protective and healing properties. For example, Li et al. found that human umbilical cord mesenchymal stem cells-derived EVs attenuate inflammation and M1 microglia polarization, thereby significantly reducing neurological damage through targeting cholesterol-25-hydroxylase (CH25H) and inactivating the Toll-like receptor (TLR) pathway (Li et al. 2020). Microglia have also been linked to this (Li et al. 2022). For instance, microglia have been shown to enhance cell-cell interaction in the treatment of stroke through a variety of pathways, most notably by the production of EVs. M2 microglial EVs can inhibit the development of glial scars, decrease neuronal autophagy and apoptosis, and enhance angiogenesis, making them a promising option for novel stroke therapy (Liu et al. 2021; Song et al. 2019; Tian et al. 2019; Zhang et al. 2021). Moreover, in ischemic stroke mice, EVs from hypoxia-preconditioned microglia could increase angiogenesis and suppress apoptosis via the TGF-beta 1 (TGF-1)/Smad2/3 pathway (Zhang et al. 2021a).

1.8 Aim of the thesis

Despite extensive research on ischemic stroke throughout the past years, it is still unknown what is the best way to slow down or even stop the disease progression. The main reason is that ischemic stroke pathophysiology is still largely unknown because of its protracted course and complicated etiology. As a result, ischemic stroke can only be treated with conventional drugs or interventions that primarily treat symptoms, but do not result in a final cure. In the peri-infarct region, reactive astrogliosis and perivascular AQP4 depolarization manifest and persist for a considerable amount of time. Importantly, it was revealed recently that inhibition of AQP4 can hasten neurological recovery by lowering early-stage brain edema and AQP4 depolarization as well as peri-infarct astrogliosis during the stroke. It is interesting to note that recent research in our lab has proposed a novel mechanism of action for EVs from OGD-preconditioned microglia to support tissue regeneration and neurological recovery in a stroke model in mice (Zhang et al. 2021a). However, it is currently unknown how reactive astrogliosis and the loss of AQP4 polarization can be modulated by EVs from hypoxic microglia to aid in the restoration of brain function. Given that the anti-inflammatory effects of M2 microglia and the therapeutic effects on promoting poststroke neurological function recovery could be mediated by EVs from hypoxic microglia and M2 microglia, it is reasonable to hypothesize such EVs may regulate the pathogenesis of inflammation and participate in suppressing AQP4 depolarization and astrogliosis. Therefore, we hypothesize that peri-infarct astrogliosis and AQP4 depolarization are suppressed by hypoxic microglia-derived EVs in the stroke mouse brain.

2. Materials and Methods

2.1. Chemicals, consumables and lab equipment

Table 1: Chemicals used in this study

Chemical	Product number	Manufacturer
Dimethyl Sulfoxide	2380.1000	CHEMSOLUTE®, Th. Geyer GmbH & Co. KG, Renningen, Germany
DNase I	11284932001	Sigma-Aldrich Chemie GmbH, Taufkirchen, Germany
Dulbecco's Phosphate Buffered Saline	D8537-500ML	Sigma-Aldrich Chemie GmbH, Taufkirchen, Germany
Ethanol 99%	2236.1000	CHEMSOLUTE®, Th. Geyer GmbH & Co. KG, Renningen, Germany
Ethanol 100%	8.18760.2500	Merck KGaA, Darmstadt, Germany
GlutaMAXTM-I (100X)	35050-061	Fisher Scientific GmbH, Schwerte, Germany
HyClone Characterized Fetal Bovine Serum	SH30073.02	Cytiva, Freiburg in Breisgau, Germany
Penicillin-Streptomycin	15140-122	Fisher Scientific GmbH, Schwerte, Germany
Poly-L-omithine hydrobromide	SLCH2058	Sigma-Aldrich Chemie GmbH, Taufkirchen, Germany
Thiazolyl Blue Tetrazolium Bromide	M5655-100MG	Sigma-Aldrich Chemie GmbH, Taufkirchen, Germany

0.5% Trypsin-EDTA (10x)	15400-054	Fisher Scientific GmbH, Schwerte, Germany
DMEM/F12 (1:1) Medium (1X)	P04-41150	PAN-Biotech, Aidenbach, Germany
Recombinant Murine M-CSF	315-02-10UG	Peprotech, Hamburg, Germany
Lipopolysaccharides (LPS)	L3024	Sigma-Aldrich Chemie GmbH, Taufkirchen, Germany
RIPA Lysis and Extraction Buffer	89900	Thermo Fisher Scientific, Waltham, USA
Clarity Western ECL Substrate, 500 ml	1705061	Bio-Rad Laboratories GmbH, Feldkirchen, Germany

Table 2: Consumables used in this study

Consumable	Manufacturer
0.45 µm filter Filterpur S0.45	Sarstedt, Nümbrecht, Germany
6-well plates for cell culture	Sarstedt, Nümbrecht, Germany
12-well plates for cell culture	Sarstedt, Nümbrecht, Germany
24-well plates for cell culture	Sarstedt, Nümbrecht, Germany
96-well plates, flat bottom	Sarstedt, Nümbrecht, Germany
Bottle-Top-Filter with SFCA membrane, ∅ 75 mm, pore size 0.2 µm, 500 mL	Carl Roth GmbH + Co. KG, Karlsruhe, Germany
Cell culture flasks w/ ventilation cap for adherent cells (25cm2, 75 cm2)	Sarstedt, Nümbrecht, Germany
Centrifugation tubes (15 mL)	Sarstedt, Nümbrecht, Germany
Centrifugation tubes (50 mL)	Sarstedt, Nümbrecht, Germany

Glass Pasteur pipettes (150 mm, 230 mm)	Th. Geyer Ingredients GmbH & Co. KG, Renningen, Germany
Petri dishes, 100 mm	Greiner Bio-One, Frickenhausen, Germany
Pipette tips w/ filters, sterile (10 µL, 100 µL, 1000 µL)	Starlab, Hamburg, Germany
Pipette tips w/o filters (10 µL)	Starlab, Hamburg, Germany
Pipette tips w/o filters (200 µL, 1000 µL, 5000 µL)	Sarstedt, Nümbrecht, Germany
Reaction tubes (1.5 mL, 2.0 mL)	Sarstedt, Nümbrecht, Germany
Serological pipettes (2 mL, 5 mL, 10 mL, 25 mL, 50 mL)	Sarstedt, Nümbrecht, Germany
CryoPure® pipes	Sarstedt, Nümbrecht, Germany
Parafilm	Bemis NA, Neenah, USA

Table 3: Lab equipment

Instrument	Manufacturer
Accu-jet® Pro pipetting aid	Brand GmbH + Co. KG, Wertheim, Germany
Autoclave Systec VX-65	Systec GmbH, Linden, Germany
Centrifuge 5810R	Eppendorf, Hamburg, Germany
Freezer -20 °C	Liebherr, Bulle, Switzerland
Freezer -80 °C Heraeus	Fisher Scientific GmbH, Schwerte, Germany
HS18 1.8 Microbiological Safety Cabinet Class II, Thermo Heraeus	Fisher Scientific GmbH, Schwerte, Germany
Hypoxic Glovebox IBT-HGB16	Toepffer Lab Systems, Göppingen, Germany
KL 1500 LCD	Schott AG, Mainz, Germany

Multipette Plus	Eppendorf, Hamburg, Germany
Neubauer cell counting chamber	Carl Roth, Karlsruhe, Germany
Pipettes (2.5/10/100/1000/5000 µL)	Eppendorf, Hamburg, Germany
Pipetus™ pipetting aid	Hirschmann Laboratory equipment GmbH + Co. KG, Eberstadt, Germany
Refrigerator +4 °C	Liebherr, Bulle, Switzerland
Sartorius™ arium pro VF Ultrapure Water System	Sartorius AG, Göttingen, Germany
Tecan Sunrise Microplate Reader	Tecan Group AG, Mondadori, Switzerland
Thermo Scientific™ Heraguard™ Clean air workbench	Fisher Scientific GmbH, Schwerte, Germany
Thermo Scientific™ Heracell™ 150i CO2-Incubator	Fisher Scientific GmbH, Schwerte, Germany
Water Bath WNB 45	Memmert GmbH + Co. KG, Schwabach, Germany
Zeiss Axiovert 25 inverse microscope	Zeiss, Oberkochen, Germany
Zeiss Stemi 2000 ZOOM stereomicroscope	Zeiss, Oberkochen, Germany

2.2. Isolation and culture of primary microglia and astrocytes

Cortices of newborn C57BL/6 mice were used to isolate primary astrocytes and microglial cell cultures as previously described (Lian et al. 2016), with a few minor modifications. Firstly, T75 flasks were coated with 10 ml of 0.1 mg/ml poly-D-lysine (PDL) and incubated at 37 °C for at least 1 h prior to the brain dissection. The cortices were then collected in HBSS on ice after the pups were decapitated, and the meningeal layers and major blood vessels were removed. These cortices were next treated in a trypsin/EDTA solution (1% trypsin; 0.025% EDTA in serum-free medium) for 15 min at 37 °C. After that, 200 µl of 10 mg/ml DNase was used to break down the clumpy DNA that dead cells release. Following that, 15 ml tubes containing the cell suspension from 3.5 - 4.5 brains were centrifuged at 300 x g for 5 min at room temperature. The pellet was resuspended in 10 ml of warm culture media after the

supernatant had been carefully removed. To get rid of any remaining trypsin, the homogeneous cell suspension was centrifuged at 300 x g for an additional 5 min. The resulting pellet was dissolved in 20 ml of astrocyte comprehensive medium, the resulting cells were seeded in T75 flasks with 20 ml of astrocyte full medium, and the cells were cultivated in an incubator (5% CO2, 37 °C, 95% relative humidity) for 10 to 12 days with a medium change every two to three days. By rotating the culture flasks at 200 rpm for 1 h at a constant 37°C or by applying mild trypsinization for 40 min, microglia were separated from mixed glial cell cultures. In DMEM/F12 (4.5 g/L glucose) supplemented with 10% FBS, 1% GlutaMAX, and 1% Penicillin/Streptomycin, the microglia were then cultivated. By shaking the co-cultured media with the microglia at 250 rpm for 24 h at 37°C, the remanent microglia were collected. In an incubator the astrocytes were grown in DMEM (4.5 g/L glucose) with 10% FBS, 1% GlutaMAX, and 1% Penicillin/Streptomycin as supplements.

2.3. Oxygen-glucose deprivation (OGD)

The OGD was conducted to recreate hypoxic conditions in vitro. The cell seeding density of astrocytes was 450,000 cells per well for 6-well plates and 90,000 cells per well for 24-well plates. The microglia cell seeding density was 200,000 - 400,000 cells per well for 6-well plates and 10,000-30,000 cells per well for 24-well plates. The given time for the cells to adhere was approximately 24 h-36 h for microglia and 48 h-72 h for astrocytes. After reaching 80−90 % confluence, the cells were washed twice with each 800 µl DPBS per well and received 500 µl (24-wells) or 2000 µl (6-wells) of glucose-free balanced salt solution BSS0 (116 mM NaCl, 5.4 mM KCl, 10 mM HEPES, 0.8 mM $MgSO_4$, 1mM $NaH_2PO_4H_2O$, 26.2 mM $NaHCO_3$, 0.01 mM glycine and 1.8 mM $CaCl_2$, pH 7.2 -7.4). The cells were then moved into the hypoxic chamber (<0.5 % O_2, 5 % CO_2, 95% N_2, and 70% humidity at 37 °C). To end the hypoxic conditions and initiate reoxygenation, the cells were removed from the hypoxic chamber, the BSS0 was replaced by a cell culture medium and the cells were incubated for 24 h at 37 °C and 5% CO_2. Afterward, cell viability assays, immunocytochemistry staining, protein isolation, and RNA isolation were performed. Primary microglia and astrocytes were subjected to OGD for a planned time, respectively, based on the varied tolerance of cells to hypoxic injury. During that, primary cells were treated with EVs during both OGD and reoxygenation periods for the next experiments.

2.4. EV enrichment from OGD-preconditioned microglia

Primary microglia following more than passage three were grown in a complete medium (DMEM/F12 with 10% FBS and 1% penicillin/streptomycin) to 80%-90% confluence. Cells were kept for 4 h under OGD conditions, followed by 72 h of reoxygenation. The medium was then replaced by the serum-free medium. The cell culture supernatant was collected after a 24-h incubation period and centrifuged at 300 g for 10 min before being filtered using 0.22 μm pore filters (TPP Techno Plastic Products AG, Trasadingen, Switzerland) to get rid of debris and bigger vesicles. Concerning the ultracentrifugation method, the conditioned medium was then ultracentrifuged (Optima XPN-80 Ultracentrifuge, BECKMAN COULTER, Brea, California, United States) for 2 h at 110,000 g to pellet the EVs, and then for another 2 h at 110,000 g to collect and dissolve the EVs in DPBS. In this study, EVs were collected using the previously established polyethylene glycol (PEG) precipitation technique (Butovsky et al. 2014; Kuang et al. 2020; Zhang et al. 2021a). The solution of 10% PEG 6,000 (50 % by weight; Merck Group, Darmstadt, Germany) and 75 mM NaCl were used to generate the PEG precipitation mixture. The mixture was then centrifuged for 30 min at 4,500 g after being stored at 4 °C overnight. The EV pellets were then resuspended in DPBS, and collected by ultracentrifugation for 2 h at 110,000 g. Additionally, as previously described, an iodixanol gradient centrifugation was performed to purify EVs by collecting the middle fractions (Zhang et al. 2021a). The purified pellets were finally dissolved in DPBS and kept at -80 °C until further use.

2.5. Identification and labeling of EVs

We adopted TEM to detect the microstructure of EVs based on previous protocols (Peters and Pierson 2008; Zheng et al. 2021b). The Malvern Panalytical NanoSight LM10 platform was used to measure the size distribution and particle concentration of EVs. Briefly, DPBS was first used to dissolve the EV sample. Following the addition of the diluted sample (around 0.5 ml) to the NanoSight system, the screen gain was adjusted to 1.0, the camera level to 14, and the capture time to 1 min. The screen gain and detection threshold used for the detection were 10.0 and 4, respectively. Thermo Scientific's bicinchoninic acid (BCA) protein assay was used to determine the amount of protein level, and western blot analysis was used to identify the EV markers Alix, CD81, CD9, CD63, and TSG101. To investigate that the isolated EVs from hypoxia-preconditioned microglia were internalized by cultured primary astrocytes, fluorescence labeling of EVs was conducted based on a previously described method (Kuang et al. 2020; Zhang et al. 2021a). Briefly, 10 μmol/L DiI (Invitrogen,

Carlsbad, USA), a lipophilic membrane dye, was incubated with the supernatant at 37 °C for 1 h. After the isolation of DiI-labeled EVs, cultured astrocytes were treated with DiI-labeled EVs for 24 h. The cells were then fixed and dyed for further analysis.

2.6. Cell viability

Cell viability was determined using the colorimetric MTT (thiazolyl blue tetrazolium bromide, Sigma-Aldrich, St. Louis, MO, USA) test. The basic idea behind this colorimetric assay is that metabolically active cells convert yellow tetrazolium salt (3-(4,5-dimethylthiazol-2-yl)-2,5-diphenyltetrazolium bromide) to purple formazan crystals. After OGD for 2, 4, 6, and 8 h with microglia and 2, 4, 6, 8, 10, and 12 h with astrocytes, 0.5 mg/ml of MTT was applied to the cells used in the respective experimental conditions. The MTT incubation time was 3 h at 37 °C and 5 % CO_2. The colorimetric reaction was terminated by the aspiration of the media and replacement with 600 µl DMSO for solubilizing and dissolving the crystal structures during 5 min shaking at 250 rpm. The solubilized crystal solution was then transferred into a 96-well plate, and the absorbance was measured at 565 nm. Each group's cell viability was quantified, scaled against the negative control, and shown as a percent (%) with standard error of measurement.

2.7. Lipopolysaccharide (LPS) activation

Prior to analysis, LPS was added to the astrocyte culture media at a concentration of 1 µg/ml for 24 h to promote inflammatory astrocyte reactivity. Earlier study methods served as the basis for the timing and dosage (Hung et al. 2016; Zhang et al. 2018).

2.8. In vivo experimental paradigm

In accordance with the National Institutes of Health's recommendations for the handling and utilization of laboratory animals, all experiments were carried out with government permission. Charles River, Sulzfeld, Germany supplied C57BL/6 mice that were 10–12 weeks old and weighed 25–30 g. The mice were kept in a setting with a circadian rhythm and unrestricted access to food and water. The three parts of the in vivo experiments are: 1) the impact of EV treatment on reactive astrogliosis and AQP4 polarity; 2) the impact of EV treatment on neuroinflammation; 3) the impact of EV treatment on the restoration of nerve function. The experimental design is depicted in a flow chart in **Figure 2**.

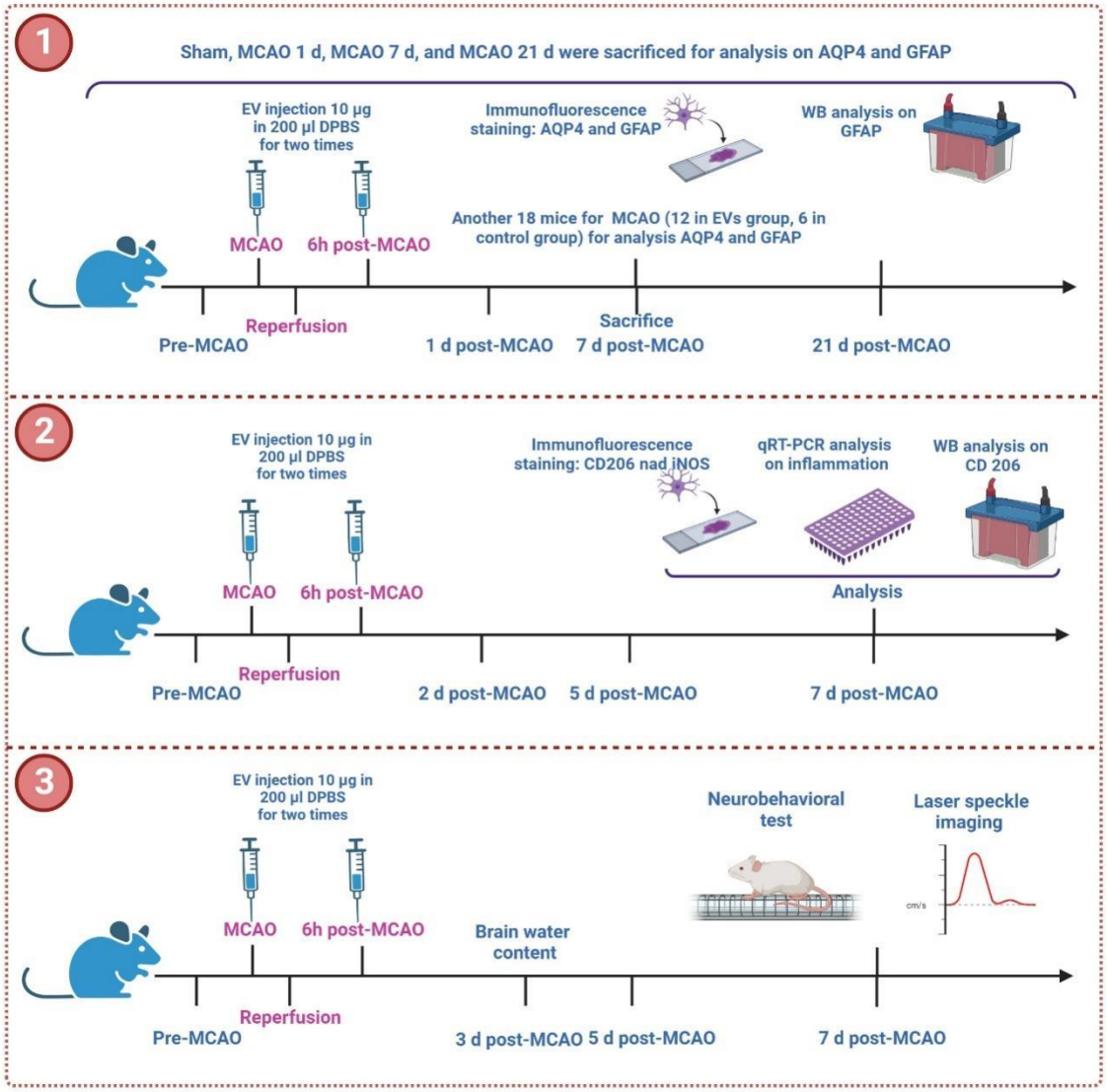

Figure 2: Flow chart of the experimental design. The three components of the in vivo experiment include the impact of EV treatment on neuroinflammation, AQP4 polarity, and reactive astrogliosis, as well as the impact of EV treatment on the restoration of nerve function.

2.7.1 The effect of EV treatment on AQP4 polarity and reactive astrogliosis

In the beginning, thirty-nine mice were divided into four groups by lot: Sham (n=9), middle cerebral artery occlusion (MCAO) 1 d (n = 9), MCAO 7 d (n = 12), and MCAO 21 d (n = 9). AQP4 polarity and reactive astrogliosis were measured 1, 7, and 21 d after MCAO for each mouse by immunocytochemistry staining (n = 5-8). Western blot analysis was used to quantify the expression of the GFAP protein in the ischemic cortex (n = 4). The 7 d group was selected for the following analysis due to the lowest AQP4 polarity. Meanwhile, another 18 mice underwent MCAO, 12 mice were arranged in the MCAO+EVs group (6 for immunocytochemistry staining and 6 for western blot), and 6 mice were randomized to the MCAO+DPBS group (all for western blot).

2.7.2 The effect of EV treatment on neuroinflammation

For the quantitative real-time PCR analysis, 6 mice were randomly divided into the MCAO+EVs group (n = 3/group) and the MCAO + DPBS group (n = 3/group). Additionally, utilizing the aforementioned slices and protein samples, immunofluorescence labelling and western blot were utilized to assess the polarization of microglia.

2.7.3 EV treatment on the restoration of nerve function

Twenty-two mice were allocated to the following three groups, at random: Sham (n = 4/group), MCAO+DPBS (n = 9/group), and MCAO+EVs group (n = 9/group). On day 7 after MACO, each mouse underwent the neurobehavioral test and laser speckle imaging. At the same time, the detection of brain water content was performed in this section (n = 9/group).

2.9. Middle cerebral artery occlusion and EV administration

As was already stated, the MCAO mouse model was used to induce focal ischemia (Zhang et al. 2021a). Briefly, C57BL/6 mice were anesthetized using 0.8 L/min of oxygen and 2.0% to 2.5% of isoflurane. To lessen the pain from the procedure, buprenorphine (0.1 mg/kg body weight) was administered around 30 min before the MCAO and once more eight hours later, and carprofen (5 mg/kg body weight) was administered immediately after surgery. To keep the body temperature stable, mice were placed on a warming pad during the surgery. The right common carotid artery, internal carotid artery, and external carotid artery were then prepared after a neck incision. The internal carotid artery was then briefly occluded with a microarterial clip after the right external carotid artery and the proximal end of the right common carotid artery were tied off. The right middle cerebral artery was then blocked by inserting a 6-0 nylon silicon-coated monofilament (Doccol Corporation, MA). After 45 min of occlusion, the filament was removed, and the wound was meticulously sealed. Mice were then transferred to their home cage, which was placed on a warming pad. The same operation was performed on the mice in the sham group, but no 6-0 nylon silicon-coated monofilament was used. Based on prior work, the mice were given MCAO before receiving injections of normal DPBS and EVs (10 μg in 200 μl DPBS) into their tail veins at the beginning of reperfusion and 6 h after MCAO (Zhang et al. 2021a).

2.10. Neurobehavioral tests

Seven days after MCAO, neurological behavior evaluations such as the rotarod test, tightrope test, balance beam test, corner turn test, modified Neurological Severity Score (mNSS), and paw slip recording were carried out (Balkaya et al. 2013; Carter et al. 1999; Zhang et al. 2021a). To ensure adequate test behavior, the mice were trained on days 1 and 2 prior to the induction of MCAO. The balance and coordination deficiencies of mice were measured using a rotarod test with escalating velocity. The test was performed for a maximum of 300 seconds, or until the mice fell off the rotarod. The balance beam test was used to evaluate gross vestibulomotor function. A mouse had to maintain balance on a 120 cm-long raised beam (50 cm above the floor). With a maximum assessment duration of 60 seconds, the mouse was perpendicularly positioned on the beam's center and the time was measured from that point until the mice reached the platform. The sensorimotor function can be assessed using paw slips. When training a mouse to cross a beam, the number of paw slips was counted. A corner test was performed by counting the number of each turn direction in front of the corner made by 2 cardboards, and finally, calculating the right turn ratio. A scale of 0 to 18 was used to score the mNSS (no deficit score, 0; maximal deficit score, 18). A more serious injury was associated with a higher score (Jin et al. 2014). The outcomes of the tightrope test were assessed using a validated score that ranged from 0 to 20 (Zhang et al. 2015).

2.11. Laser speckle imaging for cerebral perfusion analysis

Using laser speckle imaging through the skull, the CBF of mice in each group was measured on day 7 after the stroke. First, while under anesthesia, the mouse's skull was completely exposed. The focal and oblique sides' cerebral blood flow was assessed. The skin was meticulously sutured and cleaned after the measurement. Every analysis was performed in the same region of interest (ROI) position and size while simultaneously analyzing the average measured data.

2.12. Brain water content

Using a previously reported methodology, the water content of brain tissue was measured (Gao et al. 2017; Su et al. 2014). Mice were sacrificed and brain tissues were removed, weighed, and recorded in a tiny dish as the wet weight. The tissues were then dried for 48 h at 70 °C, weighed again, and recorded as the dry weight. The formula used to determine the brain water content was (wet weight dry weight)/ (wet weight) x 100%.

2.13. Immunohistochemistry and immunocytochemistry staining

The mice were transcardially perfused with 4% paraformaldehyde (PFA). The brains of the mice were separated, post-fixed in 4% PFA for 24 h, dried with 30% sucrose, and processed in 16 µm cryostat slices. On glass-bottom imaging dishes, primary astrocytes and microglia were plated before being fixed with 4% PFA at room temperature for 20 min. The brain sections were blocked with buffer containing 2% BSA blocking solution, 10% donkey serum (DS), and 0.25% Triton X-100 in tris buffered saline (TBS). The cell samples were blocked with buffer containing 10% DS and 1% BSA blocking solution in phosphate-buffered saline solution with Tween detergent (PBST). The brain sections and cell samples were then treated with the designated primary antibodies overnight at 4 °C in primary antibody diluent (**Table 4**). The slices or cells were then washed three times in DPBS before being exposed to the appropriate secondary antibody for 1 h at room temperature. Additionally, DNA in cell nuclei was stained for 10 min at room temperature with 4, 6-diamidino-2-phenylindole (DAPI, 1:10,000; AppliChem, Darmstadt, Germany).

Table 4: Antibody information for immunofluorescence staining

Antibody	Concentration	Supplier	Cat. No.	Species
Anti-CD68	1:250	BioRad	MCA341F	rat
Anti-Iba1	1:250	WAKO	011-27911	rabbit
Anti-CD11b	1:250	Abcam	ab75476	rabbit
Anti-CX3CR1	1:250	Thermo Fisher Scientific	PA5-19910	rabbit
Anti-AQP4	1:250	Abcam	ab259318	rabbit
Anti-GFAP	1:500	Millipore	AB5541	chicken
Anti-CD206	1:250	Abcam	ab64693	rabbit
Anti-iNOS	1:250	Abcam	ab15323	rabbit

2.14. Evaluating AQP4 polarity

AQP4 polarity was evaluated using a previously published protocol (Kress et al. 2014). In brief, the ROI's median immunofluorescence intensity was calculated. The percentage of the area (AQP4% Area) where AQP4 immunofluorescence was greater than or equal to perivascular AQP4 immunofluorescence was determined using the threshold analysis. The percentage of the area with lower AQP4-immunoreactivity than the perivascular astrocytic endfeet was used to represent "polarity" (i.e., "Polarity" = 100%-AQP4% Area). Of note, the 'polarity' is a relative exhibition of AQP4 localization. Herein, an increased polarity represents a higher perivascular AQP4-immunoreactivity relative to the lower parenchymal AQP4-immunoreactivity, conversely, a reduced polarity shows a lower perivascular AQP4-immunoreactivity relative to a higher parenchymal AQP4-immunoreactivity.

2.15. Western blot

Cell samples were lysed in a radioimmunoprecipitation assay lysis buffer (RIPA, Thermo Fisher Scientific, Waltham, Massachusetts, USA) on ice for 30 min with gentle agitation. Then cell lysates were centrifuged at 10,000 g for 10 min. The ischemic cortex and the surrounding penumbra tissue were collected in cold DPBS on ice and fully homogenized in RIPA buffer. BCA protein assay kit (Pierce, Rockford, IL, USA) was employed for the detection of protein concentration. Then 10% SDS-polyacrylamide gel electrophoresis (SDS-PAGE) was used to separate proteins based on their molecular weight. After the electrophoresis, proteins were further transferred onto a nitrocellulose membrane (Bio-Rad, Hercules, California, USA). Following the transfer, the membrane was blocked with 5% milk dissolved in tris-buffered saline solution with 1% Tween-20 for 1 h at room temperature. The membrane was incubated with secondary anti-chicken, anti-mouse, or anti-rabbit-antibody (1:10,000 dilution) at room temperature for 1 h after being incubated with primary antibodies for an overnight period at 4°C and being washed three times with tris-buffered saline solution containing 1% Tween-20. Finally, using the imaging device ChemiDocTM XRS+, protein signals were produced after being submerged in ECL reagent (Bio-Rad). The information primary antibodies are listed in **Table 5**.

Table 5: Antibody information for western blot analysis

Antibody	Concentration	Supplier	Cat. No.	Species
Anti-Alix	1:1,000	BD Biosciences	611620	mouse
Anti-CD63	1:1,000	Biorbyt	orb11317	rabbit
Anti-CD81	1:1,000	Abcam	ab155760	rabbit
Anti-CD9	1:1,000	Abcam	ab92726	rabbit
Anti-TSG101	1:1,000	GeneTex	GTX70255	mouse
Anti-AQP4	1:1,000	Abcam	ab259318	rabbit
Anti-GFAP	1:2,000	Millipore	AB5541	chicken
Anti-CD206	1:1,000	BioLegend	141708	rabbit
Anti-β-actin	1:10,000	Abcam	ab6276	mouse
Anti-GAPDH	1:10,000	GeneTex	GTX627408	mouse
Anti-Tubulin	1:10,000	GeneTex	GTX628802	mouse
Anti-rabbit	1:10,000	Abcam	ab97051	goat
Anti-mouse	1:10,000	Abcam	ab97023	goat
Anti-chicken	1:10,000	Santa Cruz Biotechnology	sc-2428	goat

2.16. RNA isolation and quantitative real-time PCR analysis

Total RNA was extracted using the TRIzol reagent (Invitrogen, Waltham, Massachusetts, USA) according to the manufacturer's instructions. All gene expression analyses were performed by the KAPA SYBR® FAST One-Step Kit for LightCycler®480 (Merck Group, Darmstadt, Germany), according to the manufacturer's instructions. The PCR primers were purchased from Eurofins Genomics (Ebersberg, Germany), as described in **Table 6**. All the calculations for the relative expression analysis results were normalized to PPIA or β-actin using the $2^{-\Delta\Delta Ct}$ method.

Table 6: Sequence information of quantitative real-time PCR analysis primers

Gene name	Primer sequence (5'-3')
rCD206 F	CTCTGTTCAGCTATTGGACGC
rCD206 R	CGGAATTTCTGGGATTCAGCTTC
riNOS F	AGGAACCTACCAGCTCACTCTG
riNOS R	TTTCCTGTGCTGTGCTACAGTT
rIL-1β F	GCAACTGTTCCTGAACTCAACT
r IL-1β R	ATCTTTTGGGGTCCGTCCAACT
rIL-6 F	GAGGATACCACTCCCAACAGACC
rIL-6 R	AAGTGCATCATCGTTGTTCATACA
rIL-10 F	AGAAAAGAGAGCTCCATCATGC
rIL-10 R	TTATTGTCTTCCCGGCTGTACT
rTNF-α F	AAGCCTGTAGCCCACGTCGTA
rTNF-α R	GGCACCACTAGTTGGTTGTCTTTG
rAQP4 F	CCCGCAGUUAUCAUGGGAATT
rAQP4 R	UUCCCAUGAUAACUGCGGGTT
rPPIA F	GAGCTGTTTGCAGACAAAGTTC
rPPIA R	CCCTGGCACATGAATCCTGG
rβ-actin F	CGTGCGTGACATCAAAGAGA
rβ-actin R	CCCAAGAAGGAAGGCTGGA

2.17. In Vitro co-culture astrocytes-microglia communication model

To investigate how AQP4 contributes to astrocyte-microglia communication, an in vitro co-culture system of astrocytes and microglia was employed. In the upper and lower compartments, astrocytes and microglia were seeded on a microporous membrane, respectively (**Figure 3A**). Microglia were exposed to co-culture with astrocytes of different conditions because these astrocytes express different levels of AQP4 (**Figure 3B**). **Figure**

3C shows how the co-culture system was established. These astrocytes were split into three groups: normoxic astrocytes, astrocytes that had undergone 8-h OGD and subsequent 24-h reperfusion, and astrocytes that had undergone 8-h OGD and subsequent 24-h reperfusion combined with EV therapy. These astrocytes were then exposed to primary microglia for 24 h. The primary microglia's total RNA was extracted.

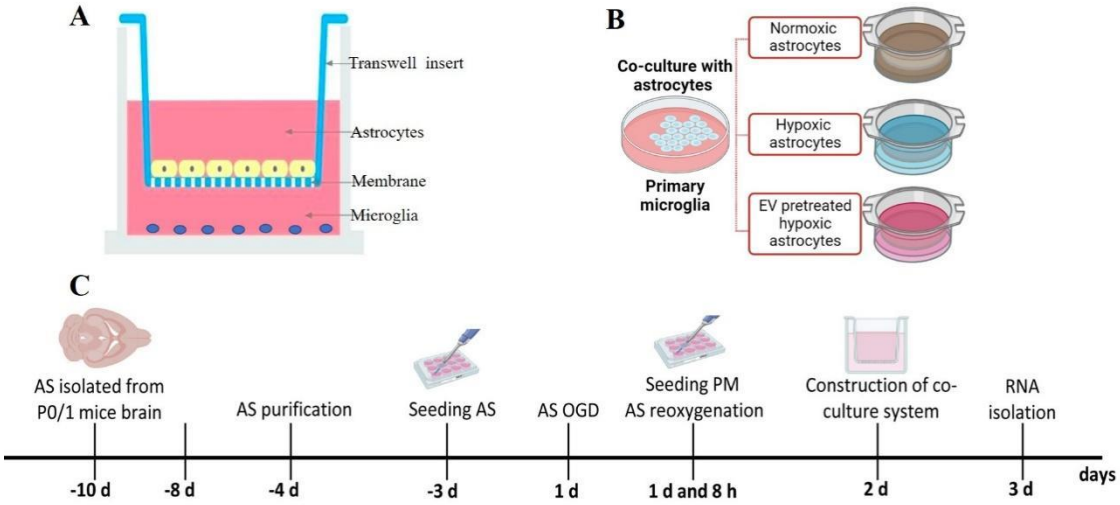

Figure 3: The establishment of the co-culture system of astrocyte–microglia communication. Astrocytes and microglia were sown on the top and lower compartment, respectively, in accordance with (A); (B) Microglia were exposed to co-culture with astrocytes under three different conditions; (C) Time line of the in vitro communication co-culture model. OGD, oxygen-glucose deprivation; AS; astrocytes.

2.18. Statistical analysis

The mean and standard error of the mean is displayed for all data. A p value of 0.05 or less was regarded as statistically significant, and GraphPad Prism 9.0 (GraphPad Software, San Diego, CA, USA) was used for data analysis and plotting. The T-test was employed to assess the significance of the comparison of two groups, and the sample comparison between multiple groups was analyzed by one-way or two-way analysis of variance (ANOVA).

3. Results

3.1. OGD shifts primary microglia to M2-type.

Microglial morphology was assessed using a light microscope (Axioplan, Zeiss, Göttingen, Germany) to identify primary microglia (**Figure 4**), and immunofluorescence technology was then used to analyze the microglia markers CD 68, CD11b, Iba1, and CX3CR1.

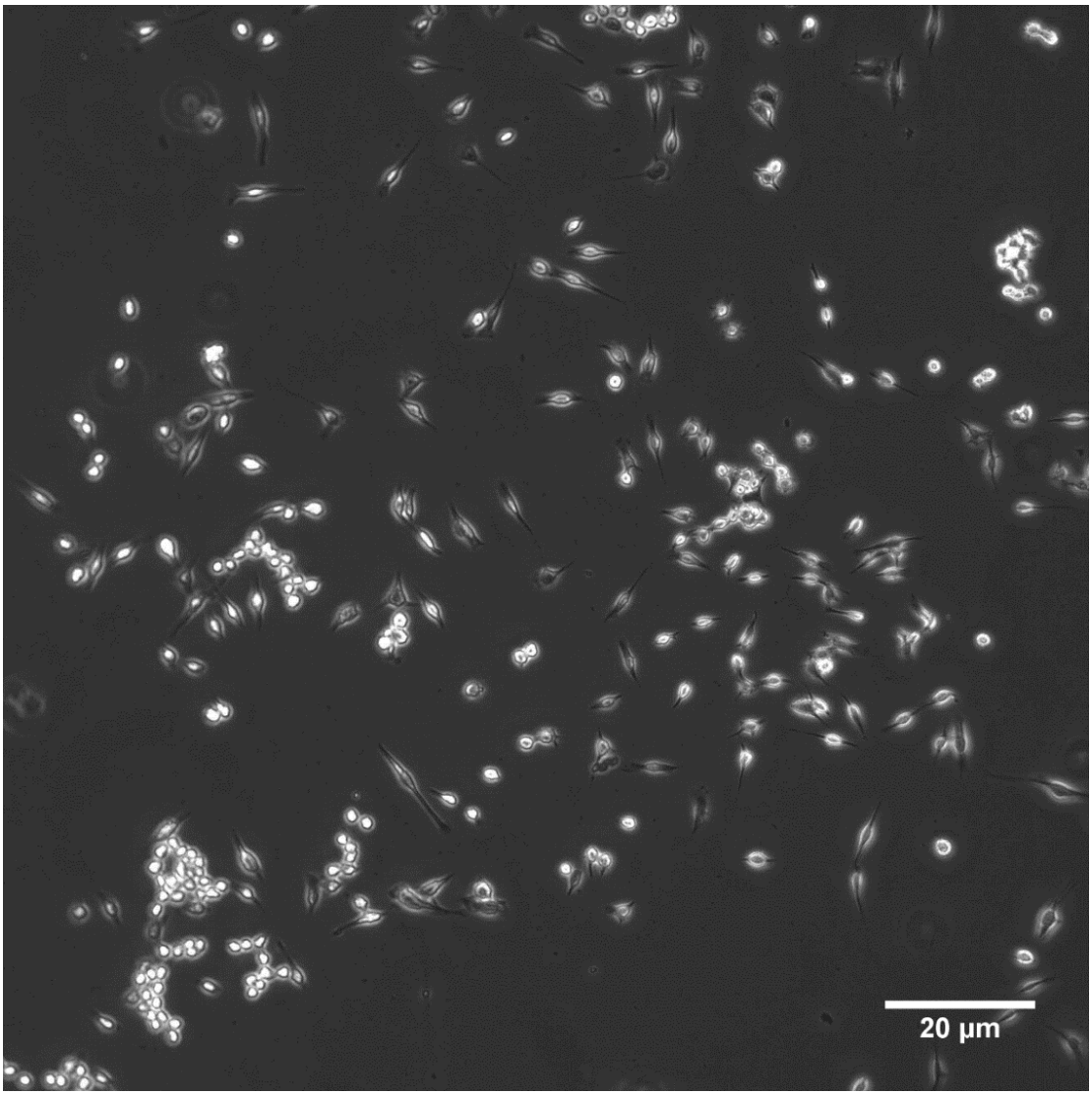

Figure 4: Light microscopy of p3 passage primary mice microglia in culture. Primary microglia were extracted from neonatal C57BL/6 mice and plated for 24 h before use. Microglia appear healthy and display the processes and a ramified morphology.

As indicated in **Figure 5**, primary microglia exhibited the typical processes and a ramified morphology. Immunofluorescence analysis displayed that the majority of cells expressed primary microglia-specific markers, namely CD68, CD11b, Iba1, and CX3CR1.

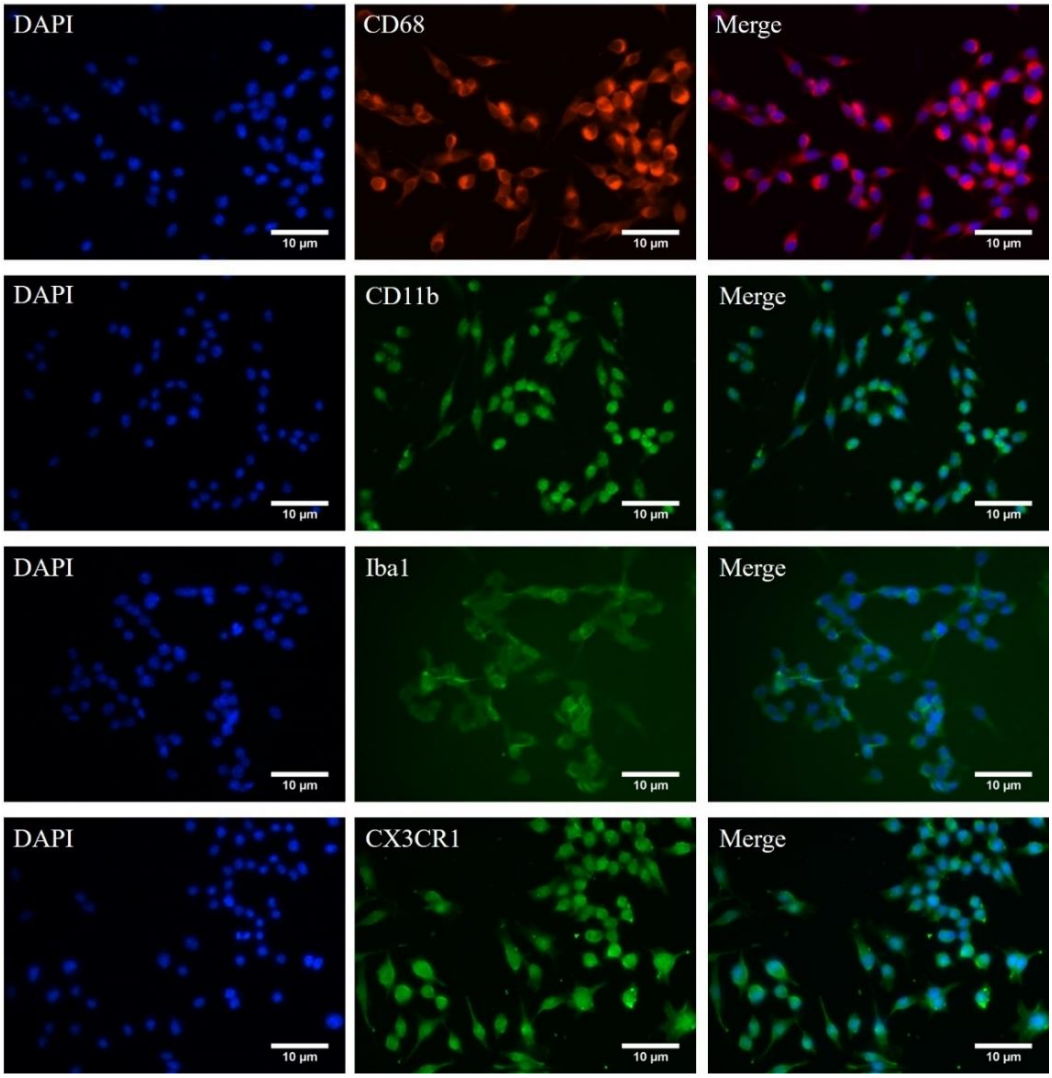

Figure 5: Identification of primary microglia. Primary microglia were extracted from neonatal C57BL/6 mice and plated for 24 h before use. Immunofluorescence staining found microglia positive for CD68 antibody, CD11b antibody, Iba1 antibody and CX3CR1 antibody. The cell nuclei were counterstained with DAPI.

Cell viability in primary microglia subjected to 2-, 4-, 6-, and 8-h hypoxia followed by 24 h of reoxygenation was examined adopting the MTT assay in five groups: normoxia, 2-, 4-, 6-, and 8-h hypoxia (n = 6). The normoxia group's cells were considered to have 100% cell survival. The 4 h OGD group achieved approximately a 50% cell viability decrease as shown in **Figure 6A**, and was selected for further analysis. Microglia were subjected to 4 h of OGD followed by various reoxygenation times in four groups: normoxia, 4-h OGD with 24-h reoxygenation, 4-h OGD with 48-h reoxygenation, and 4 h OGD with 72-h reoxygenation (n = 4). This further confirmed the impact of hypoxia on microglia polarization. The impact of hypoxia on the polarization of microglia was examined using real-time PCR. M2 type hallmark genes, such as IL-10 and CD206, were considerably upregulated in comparison to

the control group, as shown in **Figure 6B-C**. Interesting correlations were found between the length of reoxygenation (24 h, 48 h, and 72 h) and the degree of cell viability (**Figure 6D**). Together, the 4 h of OGD and the 72 h of reoxygenation were used to prepare the microglia for hypoxia.

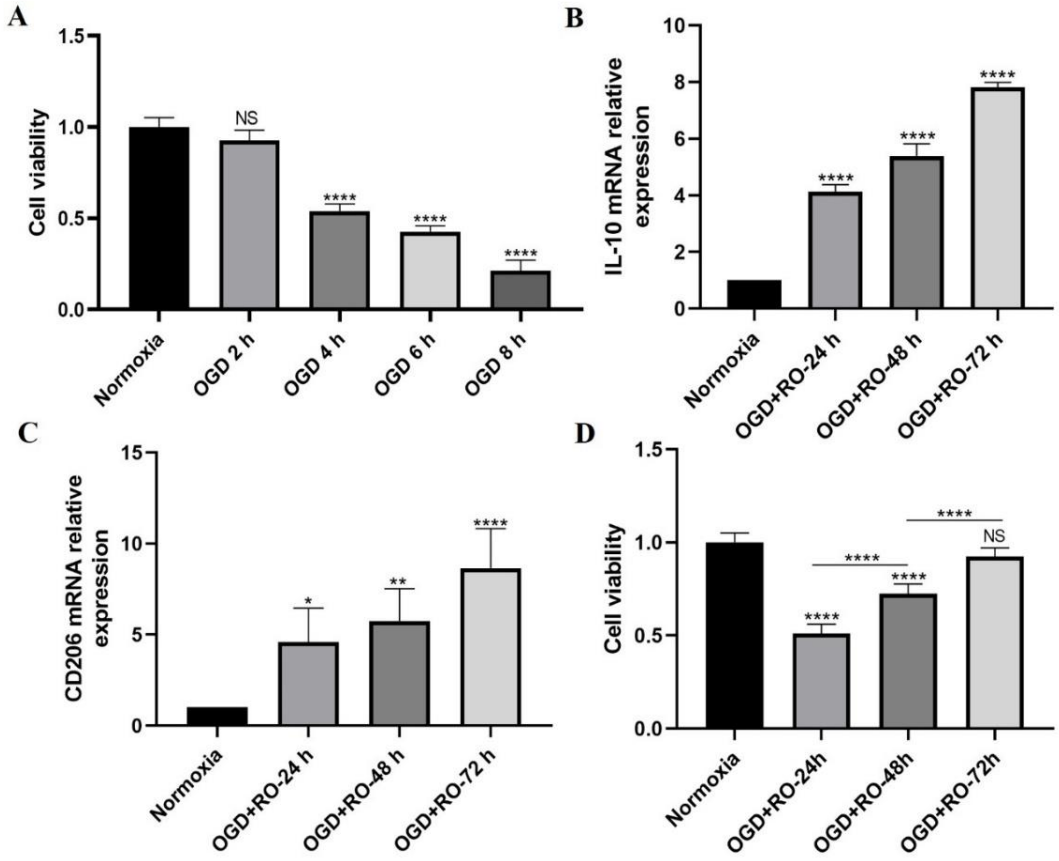

Figure 6: Oxygen glucose deprivation (OGD) activated microglia polarization towards M2 polarization.(A) Thiazolyl blue tetrazolium bromide (MTT) was used to test the microglia viability exposed to 2, 4, 6, and 8 h of OGD followed by 24-h reoxygenation (n = 6). Real-time PCR was employed to detect the M2 signature genes IL-10 (B) and CD206 (C). (D) MTT was used to test the cell viability (n = 6). *p < 0.05, **p < 0.01, ****P < 0.0001. NS, not statistically significant; IL, Interleukin; OGD, oxygen-glucose deprivation; RO, reoxygenation.

3.2. EVs from OGD microglia shift cortical microglia polarization to M2.

EVs from hypoxia-preconditioned microglia induced resting microglial polarization toward the M2 phenotype polarization, according to our prior work. Given hypoxia promotes M2 polarization, we wondered whether an increase in the concentration of EVs produced by hypoxic microglia may accelerate the M2 phenotypic polarization and inhibit M1 phenotype polarization in hypoxic microglia cells. Microglia isolated from neonatal mice were cultivated in the microglia complete medium. The cells underwent a 4-h OGD with 72-h reoxygenation.

Afterward, the serum-free medium was used in place of the complete medium to isolate EVs. EVs were captured by adopting the PEG precipitation combined with an ultracentrifugation method. A brief protocol for how EV isolation was shown in **Figure 7A**. Hypoxia-preconditioned microglia-derived EVs were verified based on the ISEV guidelines by various methods to prevent contamination with cellular components or other vesicles (Théry et al. 2018). Western blot analysis of the collected vesicular fractions revealed the presence of the typical EV markers CD9, Alix, TSG101, CD81, and CD63 (**Figure 7B**), demonstrating that these markers were present in the PEG precipitation combined with an ultracentrifugation method and the ultracentrifugation method alone. Besides that, as illustrated in **Figure 7C-D**, TEM and NTA respectively revealed that the vesicles exhibited distinct biconcave morphological features of EV (**Figure 7C**) and a diameter range from 50 to 200 nm (**Figure 7D**). Hence, these isolated vesicles were considered to be microglia-derived EVs.

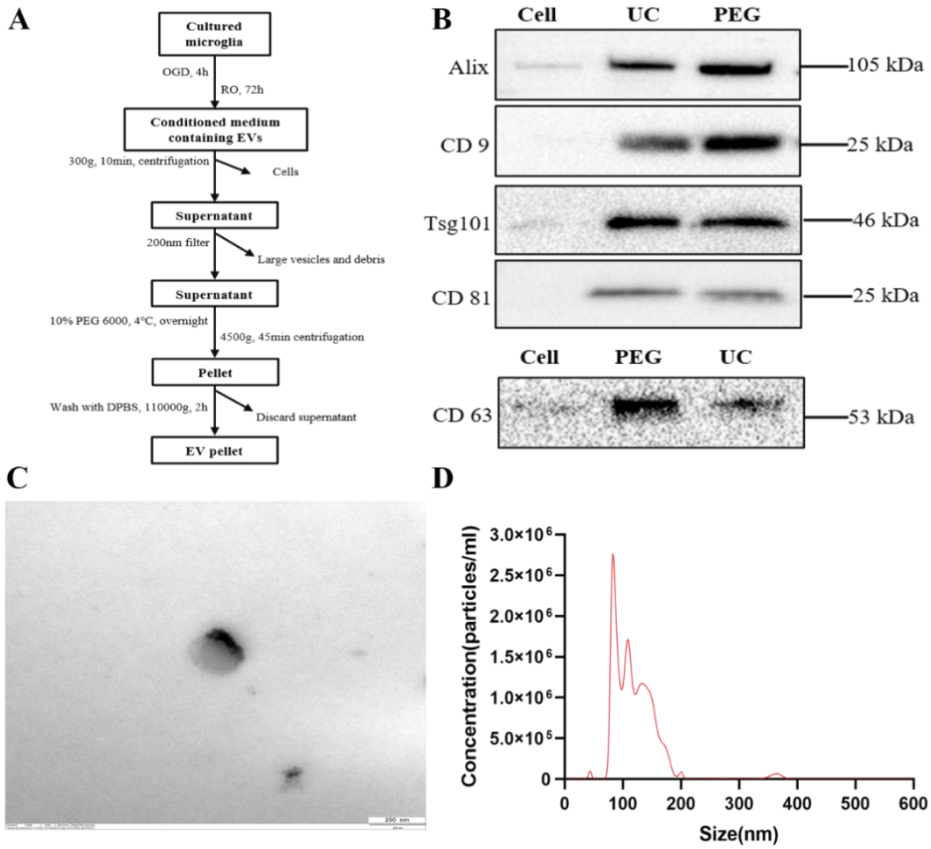

Figure 7: Isolation and characterization of EVs from hypoxic microglia. (A) To isolate EVs, conditioned media were subjected to successive polyethylene glycol (PEG) precipitation technique combined with differential centrifugation. (B) Transmission electron microscopy (TEM) analysis of vesicles derived from hypoxic microglia. (C) Vesicle size and distribution were determined using nanoparticle tracking analysis (NTA). (D) EV representative markers Alix, CD9, TSG101, CD81, and CD63 were detected by western blot. EV, extracellular vesicle; UC, ultracentrifugation; PEG, polyethylene glycol; RO, reoxygenation; OGD, oxygen-glucose deprivation; TSG101, tumor susceptibility gene 101.

After that, we looked into how these EVs affect microglial inflammation under OGD conditions. Microglia can be classified as either pro- or anti-inflammatory, depending on their level of activation. Microglial OGD-EVs enhanced the mRNA levels of IL-10 and CD206, by that inducing M2 polarization (**Figure 8A–B**). In a second step, it was investigated how EVs affected M1 polarization. After 4-h OGD with 24-h reoxygenation, the levels of iNOS, TNF-α, and IL-1β, which are produced by M1 type microglia, were increased. Our findings demonstrated that the EVs treatment group had lower production of the mRNA for the above cytokines (**Figure 8C-E**).

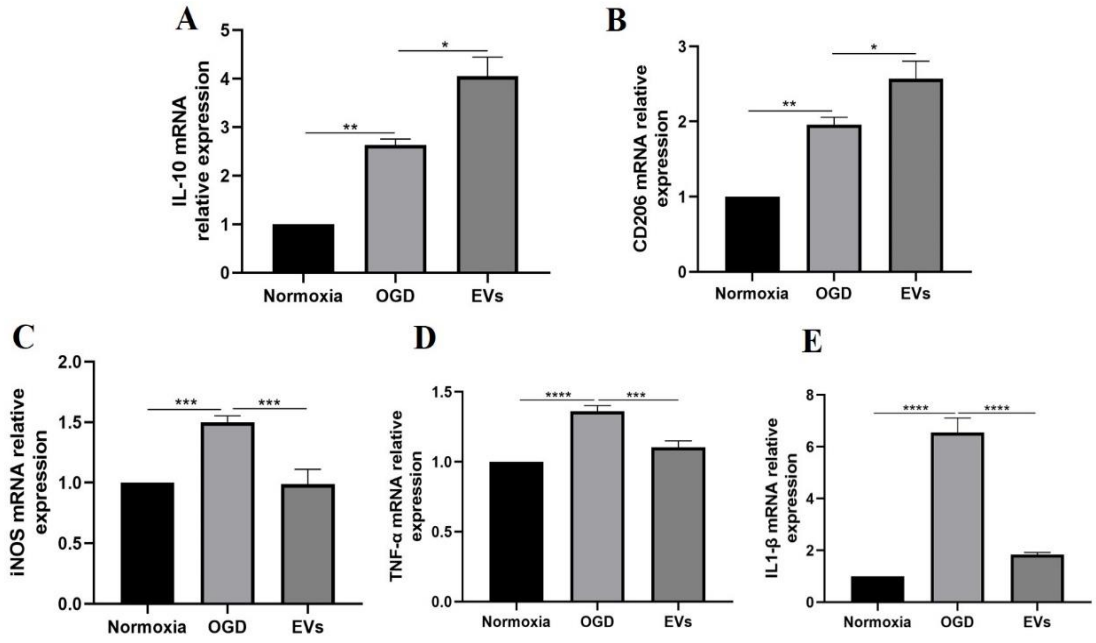

Figure 8: An increased concentration of EVs derived from OGD microglia shifts microglia polarization to M2 type. (A, B) Quantitative real-time PCR assay of M2 microglia polarization marker IL-10 and CD206 in microglia. (C-E) Quantitative real-time PCR assay of M1-associated mRNA transcripts of iNOS, TNF-α, and IL-1β in microglia. (n = 3); *p < 0.05; **p < 0.01; ***p < 0.001; ****P < 0.0001; IL, Interleukin; TNF-α, tumor necrosis factor-α; EVs, extracellular vesicles; iNOS, inducible nitric oxide synthase; OGD, oxygen-glucose deprivation.

3.3. EVs from OGD microglia abrogate AQP4 depolarization and reactive astrogliosis in the peri-infarct cortex.

Currently, studies on AQP4 polarity and stroke tend to focus more on the peri-infarct cortex (Hou et al. 2022; Sun et al. 2022). In the peri-infarct cortex, it was determined how AQP4 and GFAP were expressed. According to **Figure 9A-B**, when the polarity of AQP4 was analyzed, it was discovered that it dramatically decreased throughout the course of 1, 7, and 21 days in comparison to the sham group ($p = 0.0177$, $p < 0.0001$, $p = 0.001$). An additional

comparison was given to the time point between day 7 and day 21, the results indicated that the day 21 group uncovered a higher polarity of AQP4 ($p = 0.0124$). Moreover, measurement of the mean GFAP fluorescence intensity showed that, in comparison to sham treatment, the GFAP intensity increased on day 7 and 21 following an ischemic stroke ($p < 0.0001$, **Figure 9C**). The quantification of GFAP protein levels in the four groups is depicted in **Figure 9D**. After an ischemic stroke, the production of GFAP protein was higher in the day 7 and day 21 groups as compared to the sham group ($p < 0.0001$, $p < 0.0001$), following a similar pattern to the immunofluorescence findings. On day 1, however, there was no discernible increase in the protein expression of GFAP in the MCAO group ($p = 0.8456$).

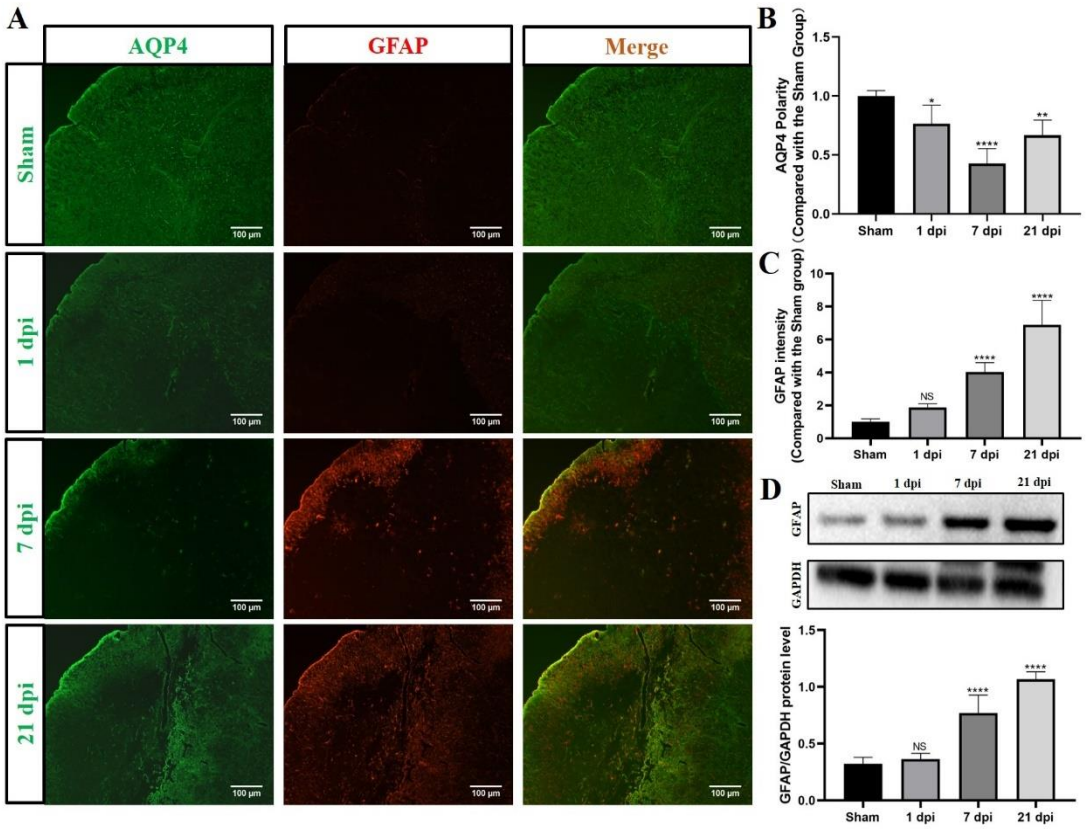

Figure 9: How the GFAP production and AQP4 polarity have changed over time in the peri-infarct brain. Fluorescence maps of AQP4 and GFAP in the cortex for several groups are shown in (A). (B, C) Statistics demonstrating the polarity of AQP4 and GFAP mean fluorescence intensity in the peri-infarct cortex of several mouse groups (n = 5-8/group). (D) The level of GFAP protein expression in the ischemic cortex (n = 4). *$p < 0.05$, **$p < 0.01$, ***$p < 0.001$, ****$P < 0.0001$; NS, not statistically significant; AQP4, aquaporin 4; dpi, day post-ischemia.

To further verify whether EVs derived from OGD microglia augment the AQP4 polarity and suppress astrogliosis in the peri-infarct brain, EVs were injected into the MCAO mouse by tail vein injection. By using AQP4 and GFAP immunostaining, it was examined how the AQP4 polarity and reactive astrogliosis in the day 7 peri-infarct cortex are affected. The

results showed that EVs from OGD microglia had an impact on the AQP4 polarity and inhibitory effects on astrogliosis that showed a lower GFAP mean fluorescence intensity ($p < 0.0001$, $p = 0.0435$, **Figure 10A-C**). The western blot was then utilized to assess how the EV treatment affected the level of GFAP protein. The trend in the level of GFAP protein was in general agreement with that of the immunofluorescence result ($p = 0.0058$, **Figure 10D-E**).

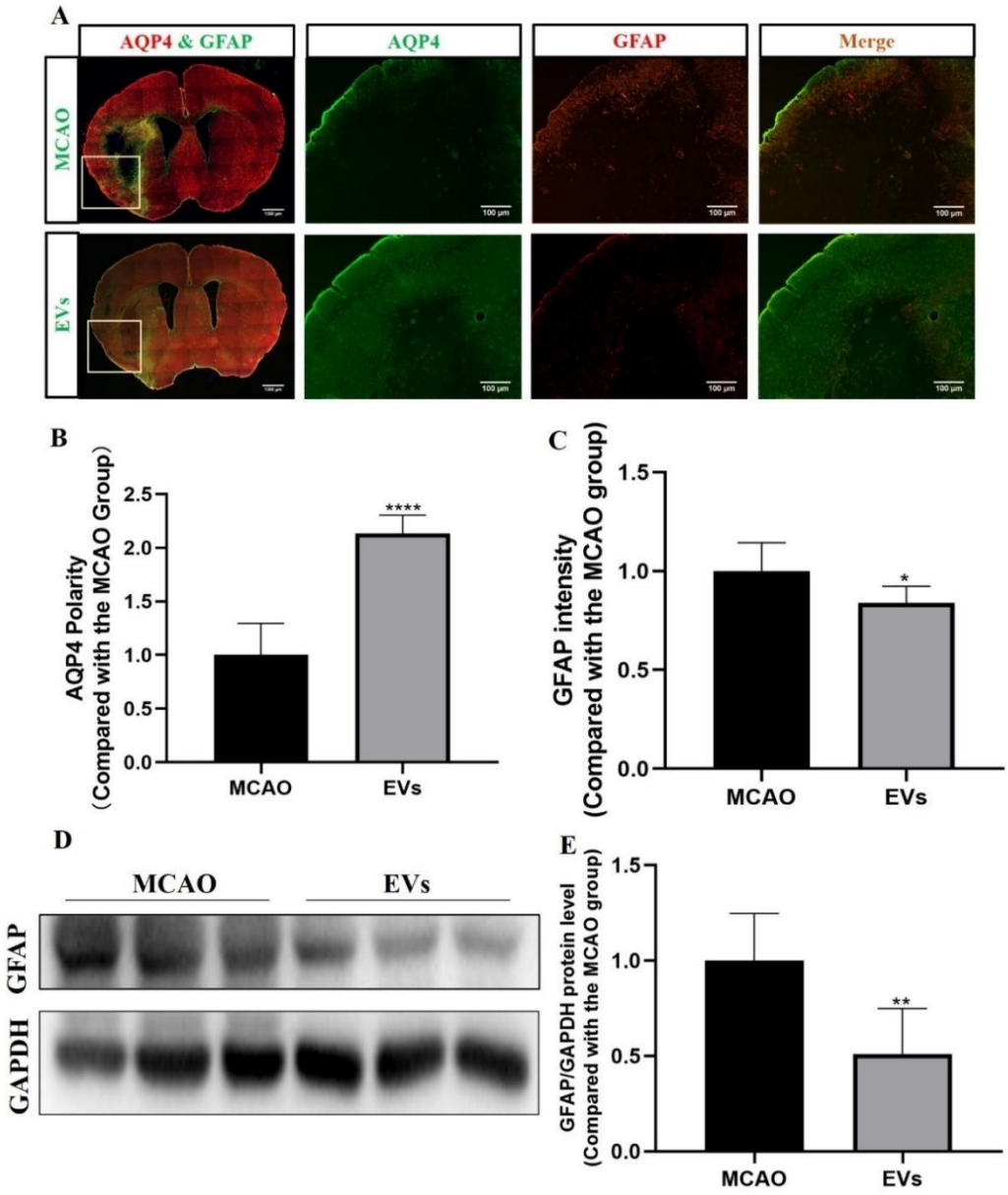

Figure 10: EVs derived from OGD microglia augmented the AQP4 polarity and attenuated astrogliosis in the one-week peri-infarct brain. (A) Detailed immunofluorescence maps and a schematic diagram of the relevant cortex. (B) The polarity of AQP4. The EV treatment group was associated with a higher AQP4 polarity ($p < 0.0001$, $n = 5$-8/group). (C) Statistical plots of the GFAP mean fluorescence intensity. The EV treatment was associated with a lower GFAP intensity ($p = 0.0435$, $n = 5$-8/group). (D, E) The GFAP protein levels in the ischemic cortex were measured by western blot ($p = 0.0058$, $n = 6$/group). *$p < 0.05$, **$p < 0.01$, ****$P < 0.0001$; MCAO, middle cerebral artery occlusion; EVs, Extracellular vesicles; AQP4, aquaporin 4.

As illustrated in **Figure 11**, the peri-infarct cortex was further divided into five regions (R), namely R1, R2, R3, R4, and R5. In such areas, the EV-administrated mice revealed fewer astrocytes by GFAP immunofluorescence staining than those in the DPBS-treated mice. In the DPBS treatment group, AQP4 was dispersed throughout the neuropil, whereas in the EV-administrated group, it was not. Under normal circumstances, AQP4 was predominately distributed in the perivascular area, which is close to the polarized distribution.

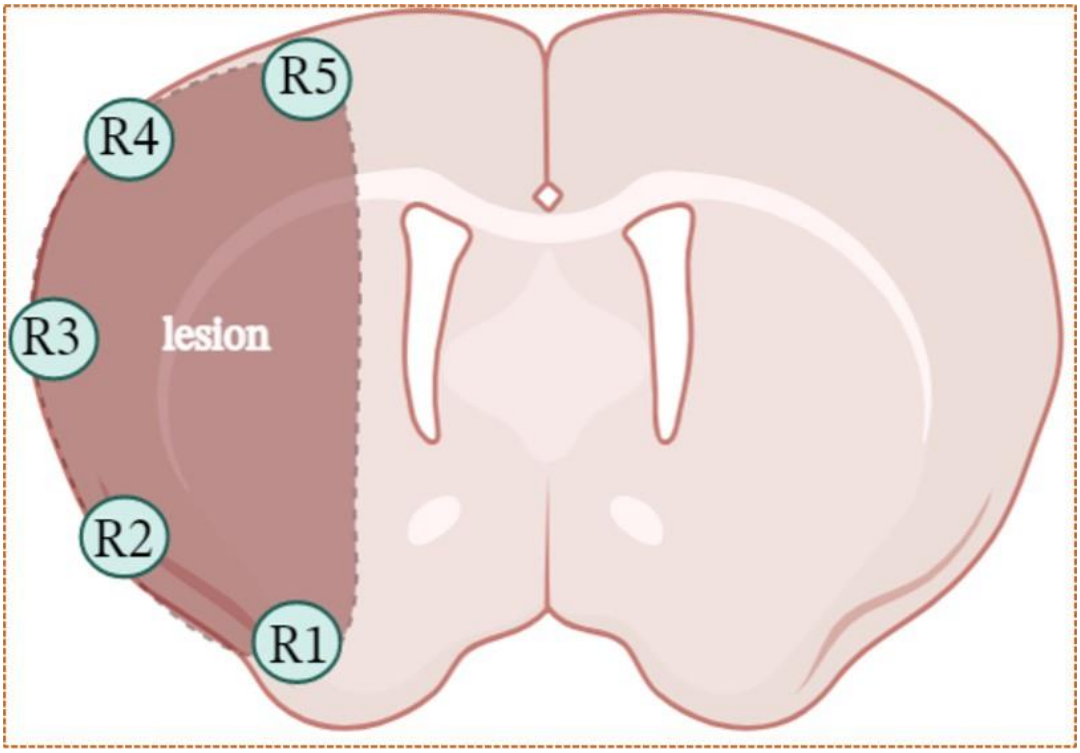

Figure 11: Schematic diagram of the division of the peri-infarct cortex. R1 to R5 indicate regions of interest.

Figure 12A shows the corresponding immunofluorescence pictures of five different areas. Quantitively, in the different areas of the cortex, the EV-administrated group exhibited a higher polarity of AQP4 in the R1, R2, R3, R4, and R5 than those of the DPBS treatment group (all $p < 0.0001$). Regarding the cortical astrocyte intensity, the EV-administrated group was associated with a lower GFAP mean fluorescence intensity in the R2, R3, and R4 ($p = 0.004$, $p = 0.0003$, $p = 0.0034$, **Figure 12B-E**), whereas the GFAP mean fluorescence intensity in the R1 and R5 was not significantly reduced ($p = 0.1497$, $p = 0.0891$, **Figure 12A, F**).

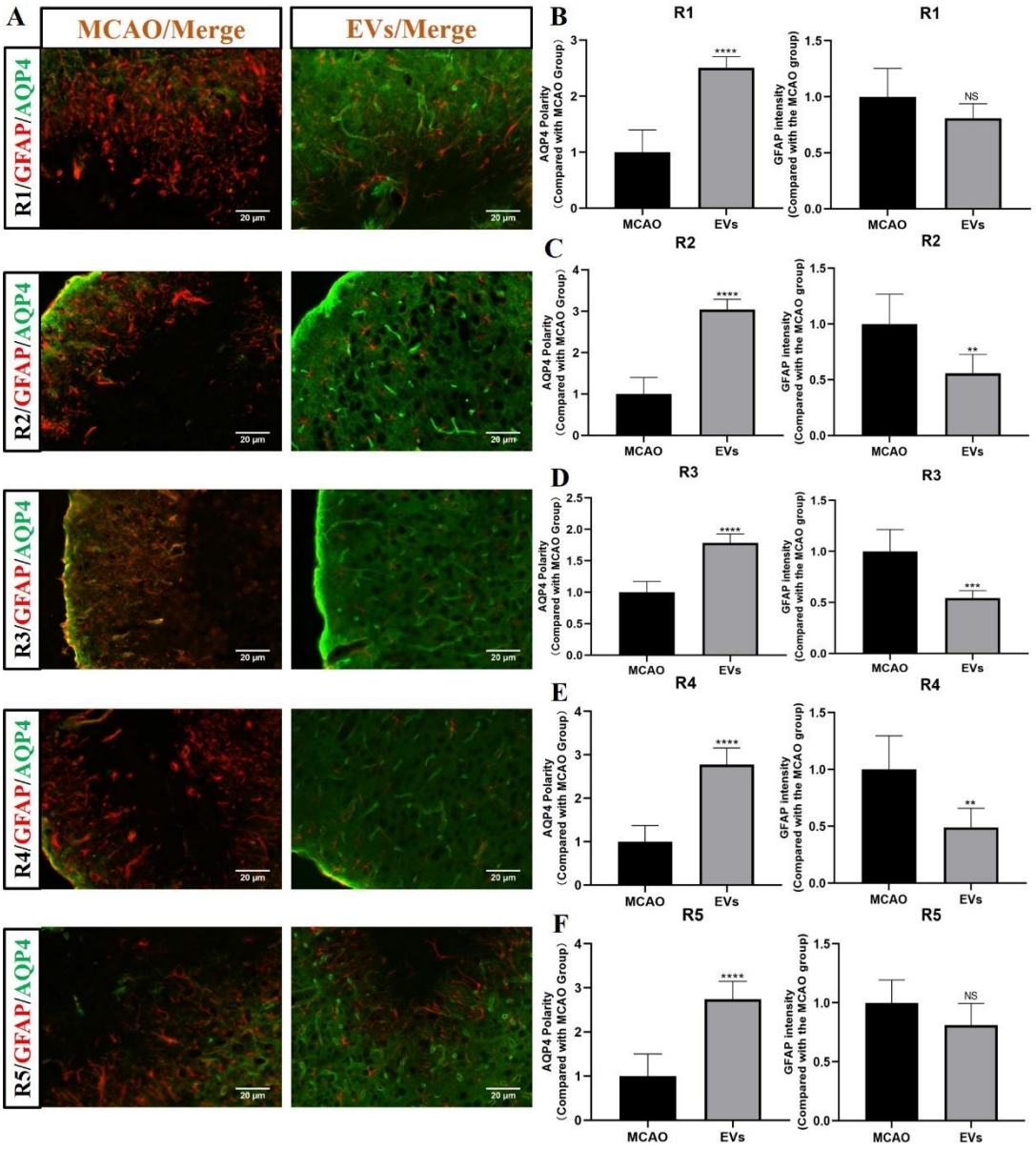

Figure 12: EVs derived from OGD microglia augmented the AQP4 polarity and attenuated astrogliosis in different regions of the peri-infarct brain.(A) Detailed immunofluorescence maps and a schematic diagram of the relevant cortex are shown. (B, C, D, E, F). The polarity of AQP4 and GFAP mean fluorescence intensity in region 1 (R1), R2, R3, R4, and R5. (n = 5-8/group). *p < 0.05, **p < 0.01, ***p < 0.001, ****p < 0.0001; NS, not statistically significant; MCAO, middle cerebral artery occlusion; EVs, extracellular vesicles; AQP4, aquaporin 4.

3.4. EVs from OGD microglia attenuate the clustering of AQP4 in the cortical astrocyte plasma membrane.

The peculiar pattern of AQP4 distribution at the astrocytic endfeet that encircle microvessels and form the glia limitans plays an essential part in the development of cytotoxic edema (Benfenati et al. 2007; Clasadonte et al. 2013). Additionally, new research using transgenic mouse models shows that AQP4 is essential for the astrocyte swelling that underlies the brain

edema brought on by pathophysiological situations including ischemic stroke (Clément et al. 2020; Manley et al. 2004). Treating astrocyte swelling is important to avoid the damaging effects of brain edema. The objective of this part was to learn more about how EVs can be used to treat stroke, by evaluating the action on the expression of AQP4 in cortical astrocytes after OGD in vitro.

Isolated primary cells had a distinctive astrocytic shape and immunostaining for the astrocyte marker GFAP, and could therefore be identified as astrocytes (**Figure 13A**). The MTT assay was adopted to test how the effects of hypoxia on astrocyte cell viability changed over time. After 24 h of reperfusion, a time effect curve was created using the results of up to 12 h. Cell viability results revealed the 8 h OGD group achieved approximately a 50% cell viability decrease as shown in **Figure 13B**, and hence this period was selected for additional study of AQP4 expression in various experimental groups.

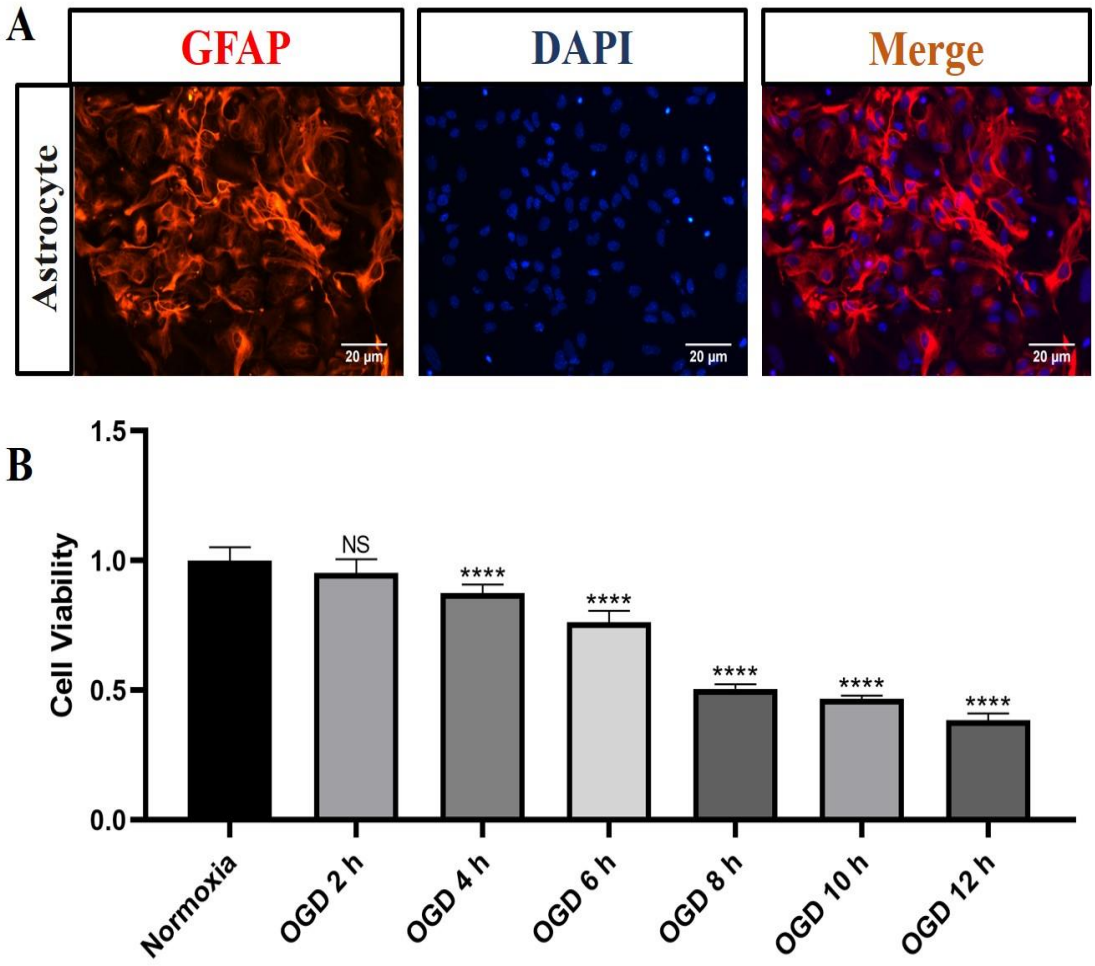

Figure 13: Primary astrocyte characterization and the effect of OGD on astrocyte viability.(A) Immunoassays against GFAP and DAPI was performed on cell cultures (blue). (B) The viability of the astrocytes subjected to 2, 4, 6, 8, 10, and 12 h of hypoxia followed by 24 h of reoxygenation was evaluated by MTT (n = 6/group). ****P < 0.0001, NS, not statistically significant.

To evaluate the impact of EVs on the expression of AQP4 in more detail, the cultured primary astrocytes were subjected to hypoxia for 8 h and further pretreated with the EVs followed by reperfusion. Upon the ischemic condition, EVs dyed red with DiI were taken up by astrocytes and stored in their cytoplasm, as shown in **Figure 14**.

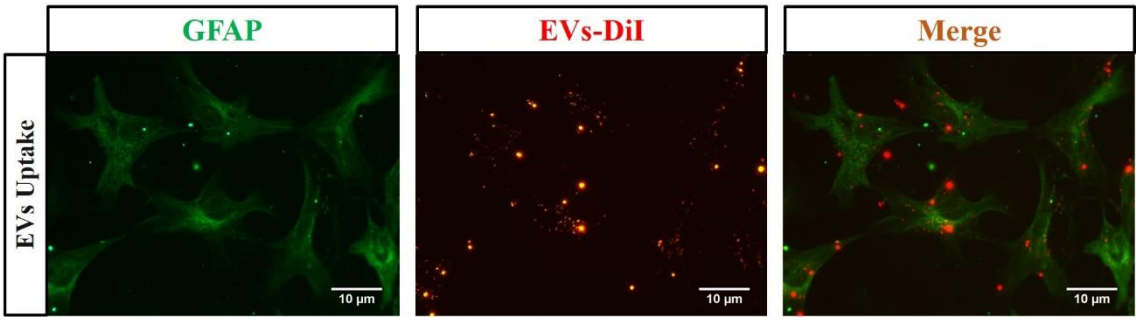

Figure 14: Astrocytes incorporated EVs dyed red with DiI into their cytoplasm.

In the next step, the aim was to verify whether primary astrocytes' increased production of AQP4 caused by OGD after reperfusion was prevented by EVs generated from hypoxic microglia. An AQP4-specific antibody was used to first measure AQP4 clustering in the plasma membrane. When compared to the normoxia group, the OGD group's astrocytes had an excessive amount of AQP4 protein aggregation ($p = 0.0001$), which was then noticeably reduced following the EV treatment ($p = 0.0053$, **Figure 15A-B**).

To analyze the changes in AQP4 gene expression, real-time PCR analysis was further employed. Notably, AQP4 expression following 8-h OGD intervention was significantly upregulated, contrasted with the DPBS treatment group ($p < 0.0001$). The EV treatment group had significantly lower AQP4 mRNA expression levels ($p < 0.0001$, **Figure 15C**), indicating an inhibitory action of the EVs.

The impact of EV therapy on astrocyte AQP4 protein expression levels during 8-h OGD followed by 24-h reperfusion was investigated using western blot analysis. After 8 h of OGD and 24 h of reperfusion, the control group's levels of astrocyte AQP4 protein expression dramatically decreased ($p = 0.0177$). **Figure 15D-E** highlights that AQP4 protein levels varied significantly in a substantial way among the EV treatment and the DPBS treatment groups ($p = 0.0004$), indicating that the EV treatment inhibits the upregulation of AQP4 expression.

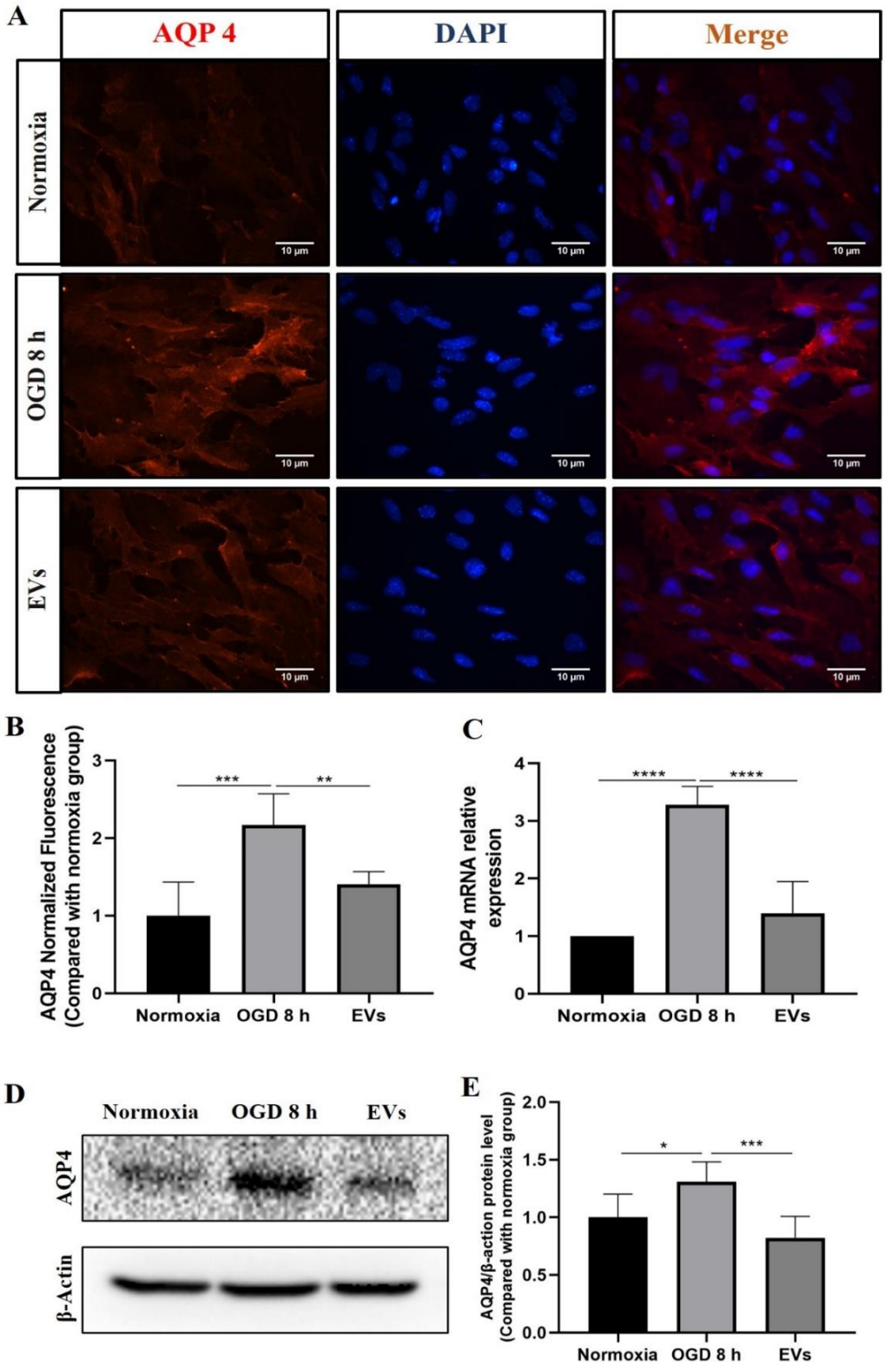

Figure 15: EV treatment decreased the clustering of AQP4 in the astrocyte cytoplasm.(A, B) Immunocytochemistry with the antibody specific for AQP4 demonstrated clustering of the protein AQP4 in the plasma membrane under various treatment conditions (n = 6/group). (C) Quantitative real-time PCR assay of the changes of AQP4 gene expression (n = 5/group). (D, E) Western blot examination of the AQP4 protein in astrocytes (n = 7/group). *p < 0.05; **p < 0.01; ***p < 0.001; ****p < 0.0001; OGD, oxygen-glucose deprivation; EVs, extracellular vesicles; AQP4, aquaporin 4.

3.5. EVs from hypoxic microglia abrogate the inflammation in cortical astrocytes challenged by hypoxia.

Astrocytes were subjected to OGD in order to further assess the influence of these vesicles produced from hypoxic microglia on the inflammation of astrocytes. OGD exposure raised the levels of pro-inflammatory molecules in comparison to normoxia. Quantitative real-time PCR was used to assess the effectiveness of the EV treatment on astrocytic inflammation, and the results showed that IL-1β, iNOS, and TNF-α mRNA levels were repressed in the EV treatment group in contrast to the DPBS treatment group (**Figure 16A-C**). However, there was no discernible change in the three groups' expression of IL-10 and CD206 mRNA (**Figure 16D-E**).

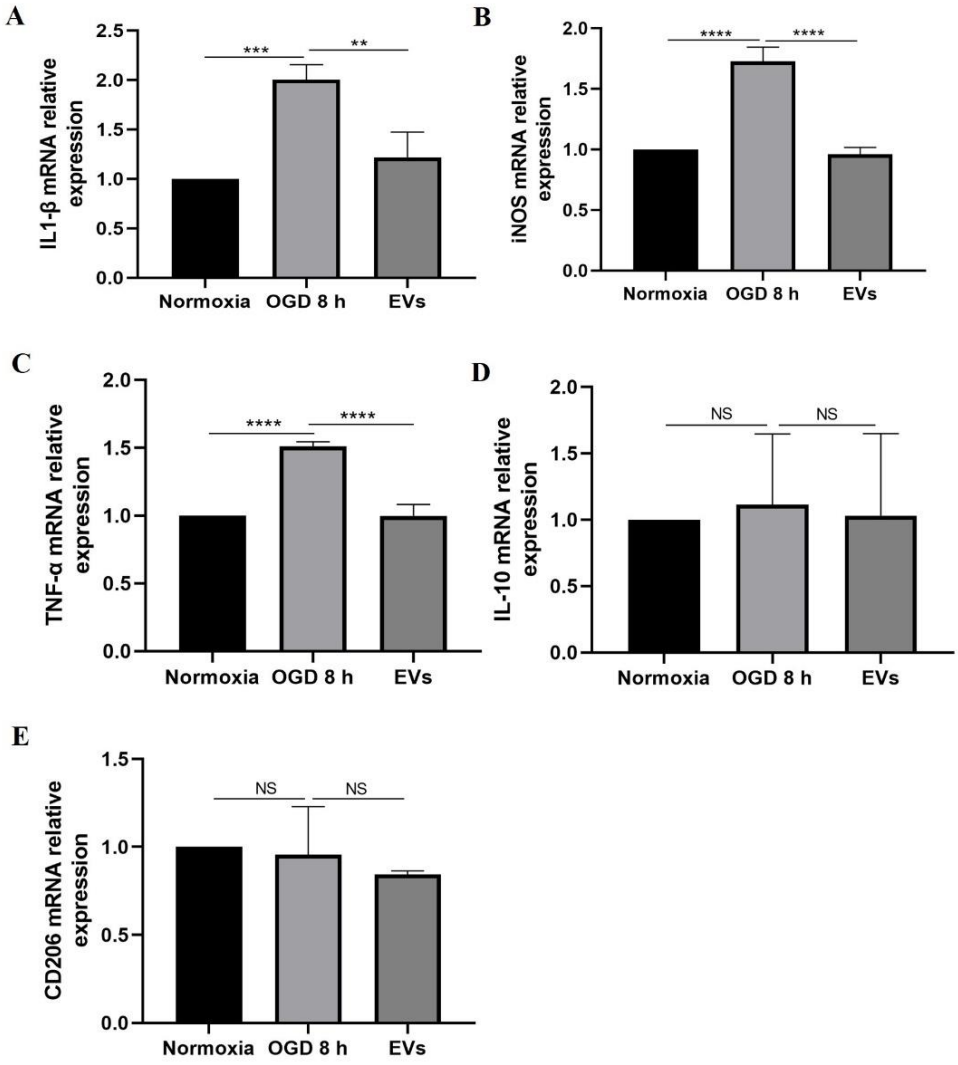

Figure 16: EVs derived from hypoxic microglia affect inflammation in hypoxic astrocytes.(A-E) Quantitative real-time PCR assay of IL-1β, iNOS, TNF-α, IL-10, and CD206 mRNA levels in astrocytes (n = 3). **p < 0.01; ***p < 0.001; ****p < 0.0001; NS, not statistically significant. IL, Interleukin; TNF-α, tumor necrosis factor-α; EVs, extracellular vesicles; iNOS, inducible nitric oxide synthase; OGD, oxygen-glucose deprivation.

To further elucidate the mechanisms of the action of EVs on inflammation, the relationship between AQP4 level and inflammation was also investigated. We first explored the effect of inflammation on AQP4 expression. Prior to analysis, LPS was introduced to the astrocyte culture media at a concentration of 1 μg/ml to stimulate inflammatory astrocyte reactivity. The LPS administration raised the production of IL-1β, iNOS, and TNF-α in comparison to the control. However, no discernible difference was identified in the AQP4 mRNA among the control and LPS groups (**Figure 17)**.

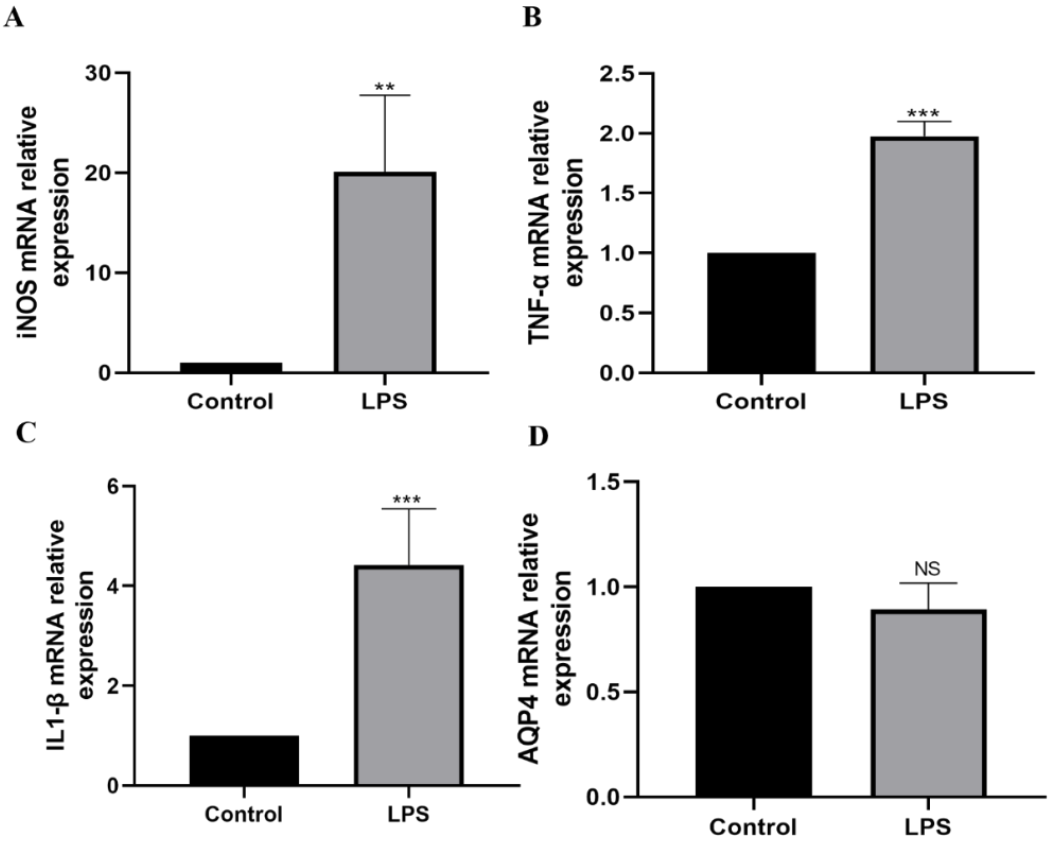

Figure 17: LPS induced inflammation but showed no impact on AQP4 level in astrocytes. (A-D) Quantitative real-time PCR analysis of iNOS, TNF-α, IL-1β, and AQP4 mRNA levels in astrocytes (n = 3). **p < 0.01, ***p < 0.001. NS, not statistically significant. IL, Interleukin; TNF-α, tumor necrosis factor-α; iNOS, inducible nitric oxide synthase; AQP4, aquaporin 4; LPS, lipopolysaccharide.

Despite AQP4 having varied functions at different phases of inflammation, there is evidence that AQP4 contributes to regulating inflammation (Dai et al. 2018; Sun et al. 2016). When astrocytes were challenged with LPS using primary astrocyte cultures obtained from $AQP4^{+/+}$ and $AQP4^{-/-}$ embryos, AQP4-deficient astrocytes produced fewer TNF-α and IL-6 (Dai et al. 2018). Moreover, as shown by Manley et al (Manley et al. 2000), a new viewpoint on AQP4's role in controlling inflammation was revealed by the fact that AQP4 deletion

reduced inflammation-related cerebral edema. However, the particular roles of AQP4 in inflammation require more investigation, particularly in the interaction between astrocytes and microglia.

Quantitative real-time PCR was adopted to quantify the inflammation-associated molecules released by microglia when they were grown alongside three different types of astrocytes. As seen in **Figure 18**, co-cultured microglial cells with astrocytes produced more IL-1β, iNOS, and TNF-α mRNA while producing less IL-10 and CD206 mRNA. Remarkably, CD206, IL-1β, and iNOS mRNA levels significantly differed following co-culture with hypoxic astrocyte, as shown in **Figure 18**, while TNF-α and IL-10 mRNA levels did not alter significantly. Notably, the findings show no discernible difference between the groups of co-culture with hypoxic astrocytes and such cells pretreated with EVs from the microglial inflammation-associated molecular levels. These results show that activated astrocytes directly reacted to activated microglia, but that alteration in the AQP4 level was unable to influence astrocyte-to-microglia communication with regard to neuroinflammation.

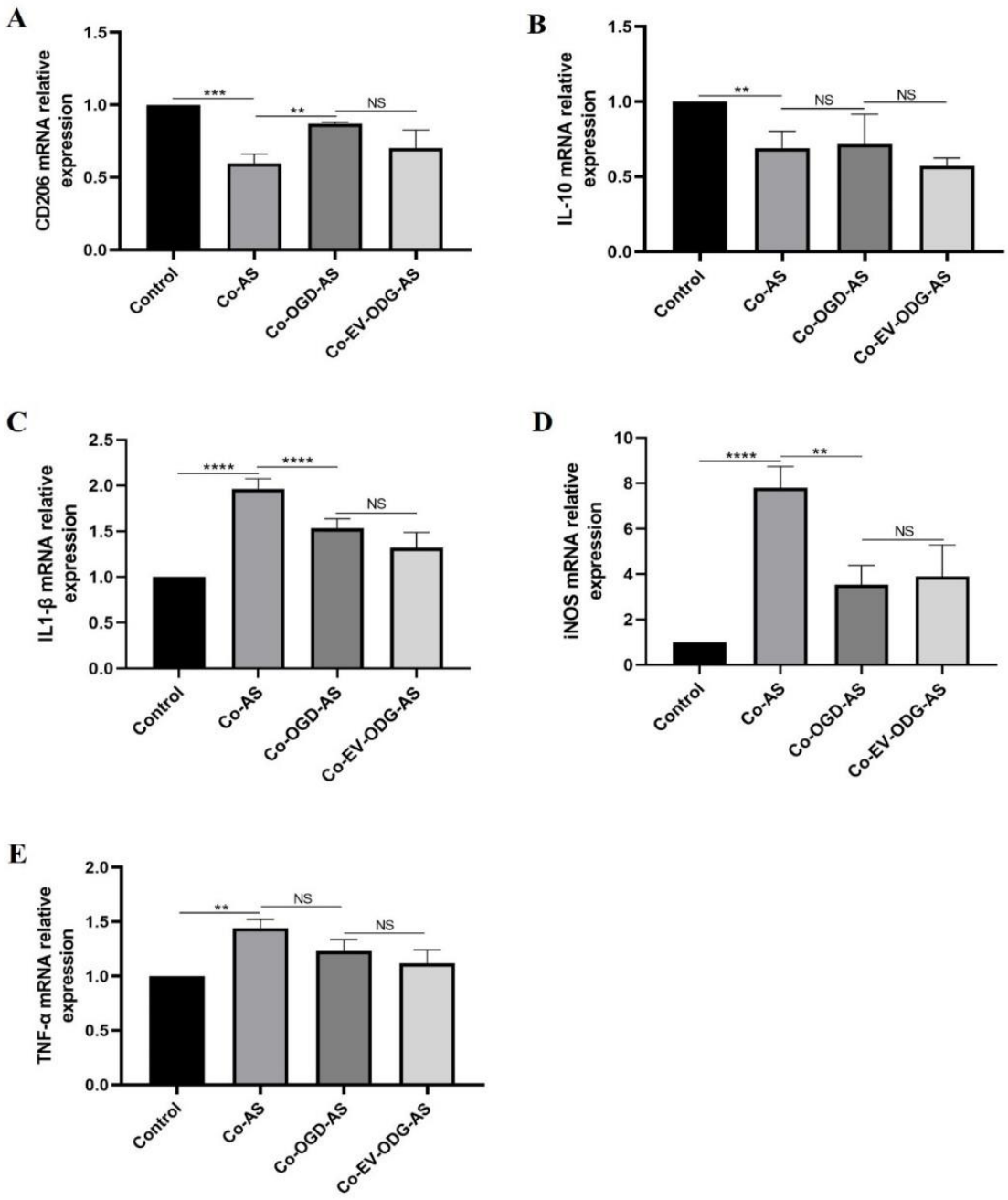

Figure 18: A change in AQP4 expression that affects how astrocytes and microglia communicate in terms of neuroinflammation. (A-E) Quantitative real-time PCR analysis of CD206, IL-10, IL-1β, iNOS, and TNF-α mRNA levels in microglia (n = 3). **p < 0.01, ***p < 0.001, ****p < 0.0001. NS, not statistically significant; OGD, oxygen-glucose deprivation; EVs, extracellular vesicles; AS; astrocytes; IL, Interleukin; TNF-α, tumor necrosis factor-α; iNOS, inducible nitric oxide synthase.

3.6. EV administration diminishes neuroinflammation in the peri-infarct cortex.

This study further questioned whether EVs affected very early inflammation in the postischemic brain given that EVs have been demonstrated to stimulate M2 microglia

polarization and reduce hypoxic astrocytic inflammation. To confirm this, the brain tissue of the peri-infarct cortex was analyzed by several methods on day 7 after MCAO. The expression of feature genes for surface markers distinguishes activated microglia. The production of the M1 marker, iNOS, was initially assessed. In the peri-infarct cortex of MCAO animal brain slices, it was strongly expressed in $Iba1^+$ cells. After the addition of EVs, the co-expression of $iNOS^+/Iba\text{-}1^+$ cells were reduced (**Figure 19A-B**). In addition, a notion was given to the levels of the proinflammatory cytokines in the peri-infarct cortex that were detected employing quantitative real-time PCR. In contrast to the DPBS treatment group, as expected, the levels of IL-1β and TNF-α mRNA decreased in the postischemic brain from EV treatment mice (**Figure 19C-D**). However, there was no discernible change in the levels of IL-6 among the two treatments. (**Figure 19E**).

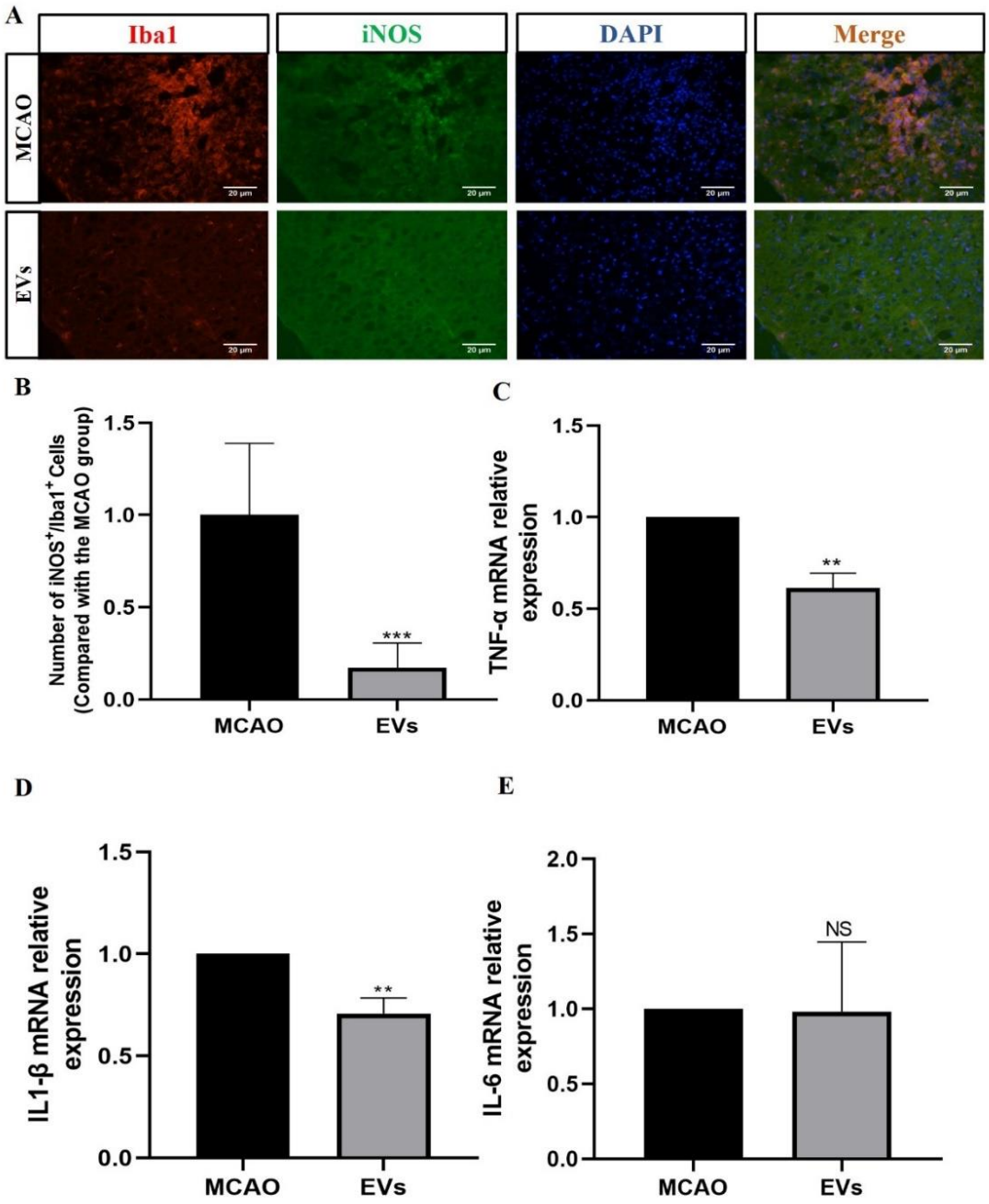

Figure 19: The pro-inflammatory factors levels. (A-B) Peri-infarct cortex is co-stained for iNOS and Iba-1 and quantification of the number of iNOS+/Iba-1+ cells (n = 6). (C-E) Quantitative real-time PCR assay of TNF-α, IL-1β, and IL-6 mRNA levels (n = 3). **p < 0.01; ***p < 0.001; IL, Interleukin; TNF-α, tumor necrosis factor-α; iNOS, inducible nitric oxide synthase; MCAO, middle cerebral artery occlusion; EVs, extracellular vesicles.

The M2 biomarker CD206 production was greater in the EV group in comparison to the MCAO group (**Figure 20A-B**). Western blot analysis supported the immunocytochemistry staining findings and revealed a similar result (**Figure 20C-D**). The findings imply that EVs affect the polarization process by favoring the M2 phenotype. In addition, a notion was given to the anti-inflammatory molecule levels, IL-10 mRNA, in the peri-infarct cortex was

assessed employing quantitative real-time PCR. In contrast to the DPBS treatment group, as expected, the expression of IL-10 mRNA increased in the postischemic brain from EV treated mice (**Figure 20E**).

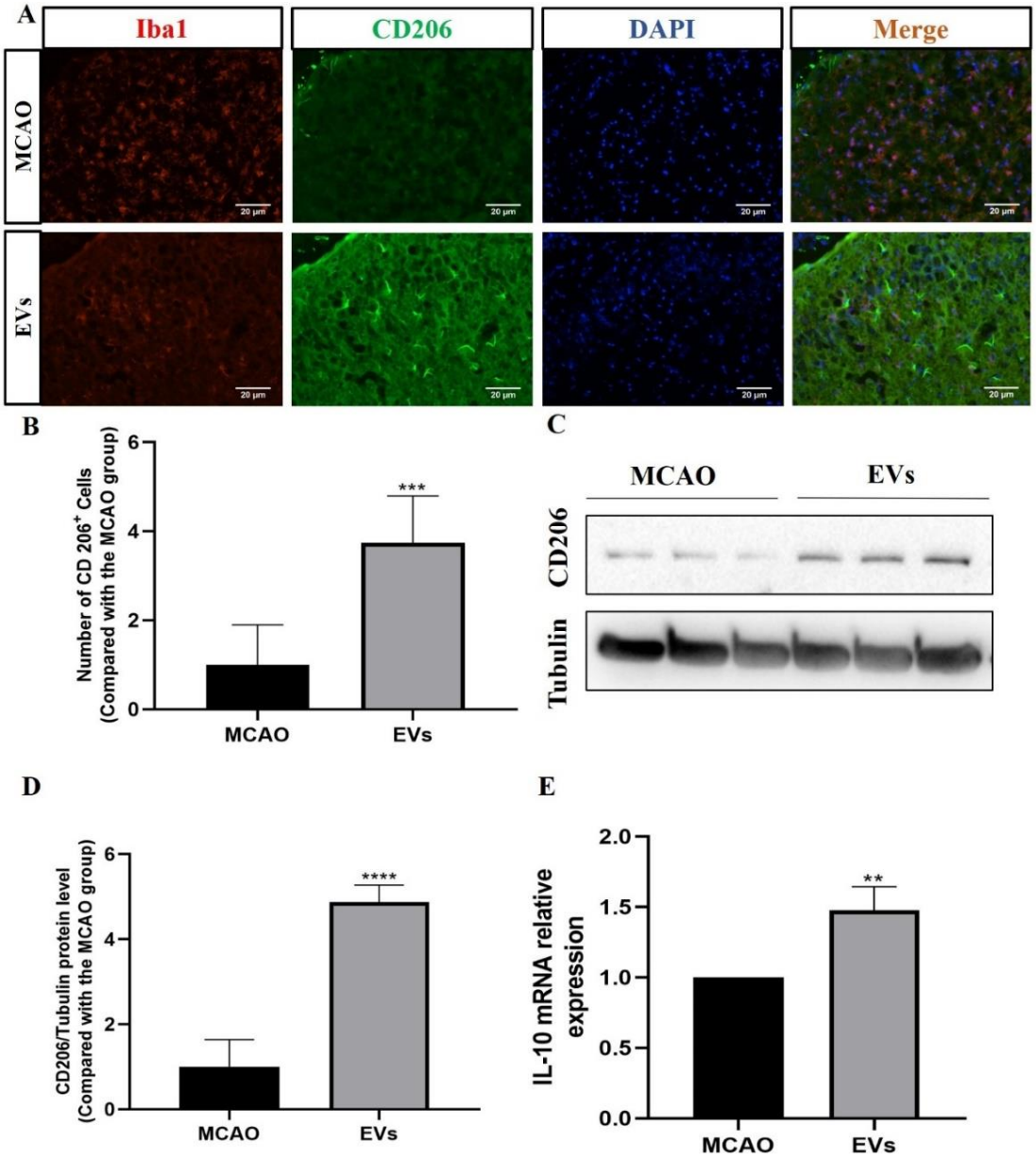

Figure 20: The anti-inflammatory factors levels. (A-B) Peri-infarct cortex stained for CD206 (M2 marker) and quantification of the number of CD206 cells (n = 6). (C-D) The CD206 protein level in the ischemic cortex (n = 6). (E) Quantitative real-time PCR assay of IL-10 mRNA levels (n = 3). ***p < 0.001; ****p < 0.0001; IL, Interleukin; MCAO, middle cerebral artery occlusion; EVs, extracellular vesicles.

3.7. EV administration protects against ischemia-induced brain damage in mice

To assess how the delivery of EVs affects brain damage after ischemia, cerebral perfusion, brain water content, and neurological function were investigated. Cortical cerebral blood flow was analyzed employing a laser speckle imager in every mouse, representative illustrations are indicated in **Figures 21A-D**. Cortical blood flow at the lesion contralateral cortex is comparable among the two treatments ($p = 0.6548$), whereas the ipsilateral cortex showed a substantial difference ($p = 0.0236$). We further analyzed the ipsilateral cortex blood flow ratio to contralateral cortex blood flow, and the result uncovered that the EV treatment group was linked to a higher value ($p = 0.0261$). The dissipation of vasogenic edema depends on perivascular polarized AQP4. The brain water content of the EV treatment group was reduced compared to the DPBS treatment group ($p = 0.0179$, **Figure 21E**).

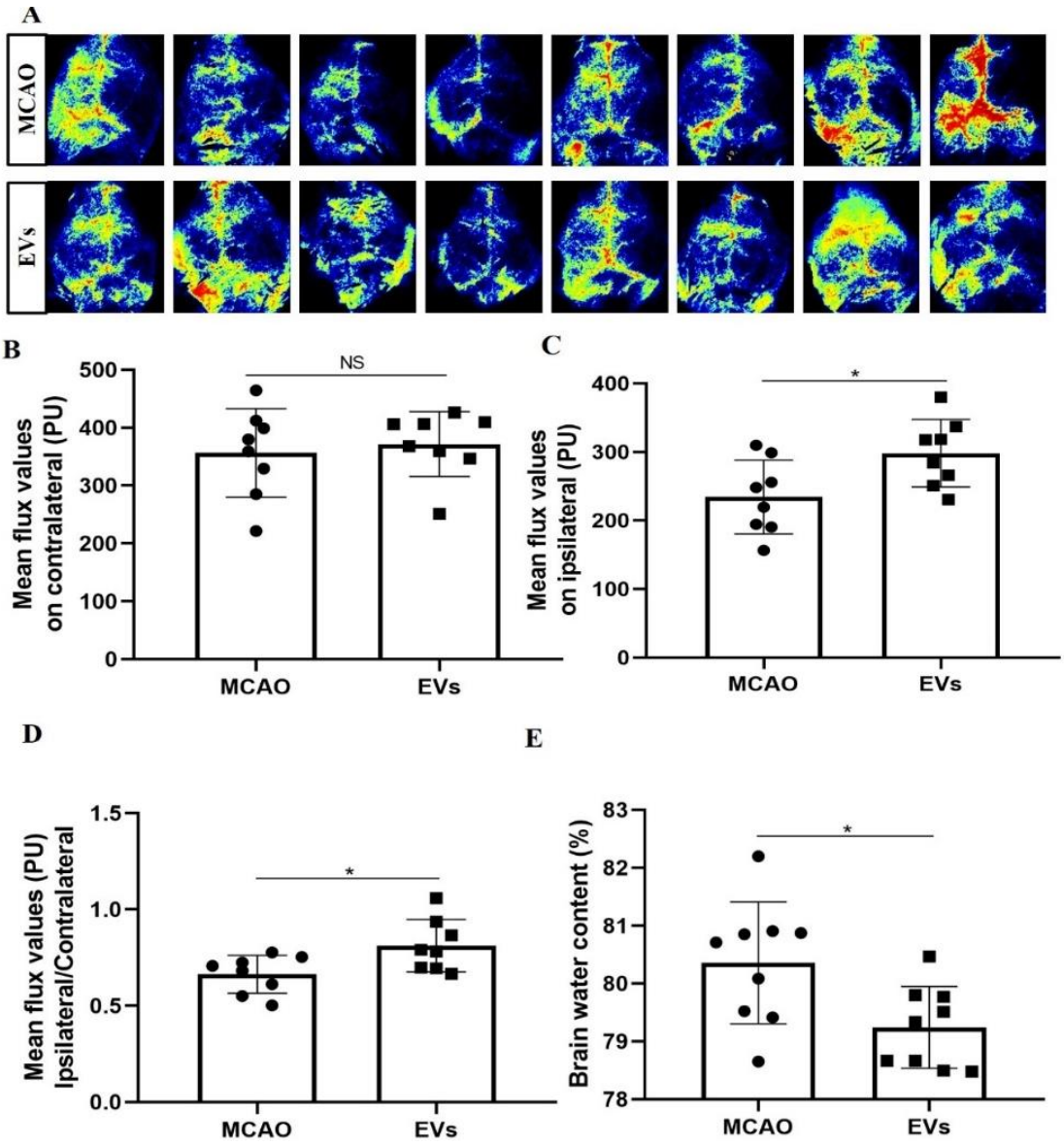

Figure 21: EV treatment improves cortex blood flow and inhibits brain edema. (A) Laser speckle imaging of all analyzed mice; (B-D) Results of blood flow in mice were statistically analyzed, n = 8/group; (E) Statistics on the water content in mouse brains, n = 9/group. *$p < 0.05$; NS, not statistically significant; MCAO, middle cerebral artery occlusion; EVs, extracellular vesicles.

In view of the above-shown data on inhibiting AQP4 depolarization, astrogliosis, and inflammation, we further explored whether, in mice with cerebral ischemia, hypoxic microglial EVs enhance neurological recovery. Neurological behavior assessments including the rotarod test, the tightrope test, the balance beam test, the corner turn test, the mNSS, and the paw slips recording were conducted on day 7 after the stroke. Supply of EVs led to noticeably better test outcomes for the mice in all of the aforementioned neurological behavior evaluations compared to the MCAO group (**Figure 22A-F**). Altogether, the behavior evaluation revealed that EV treatment significantly protected mice against postischemic motor coordination deficits.

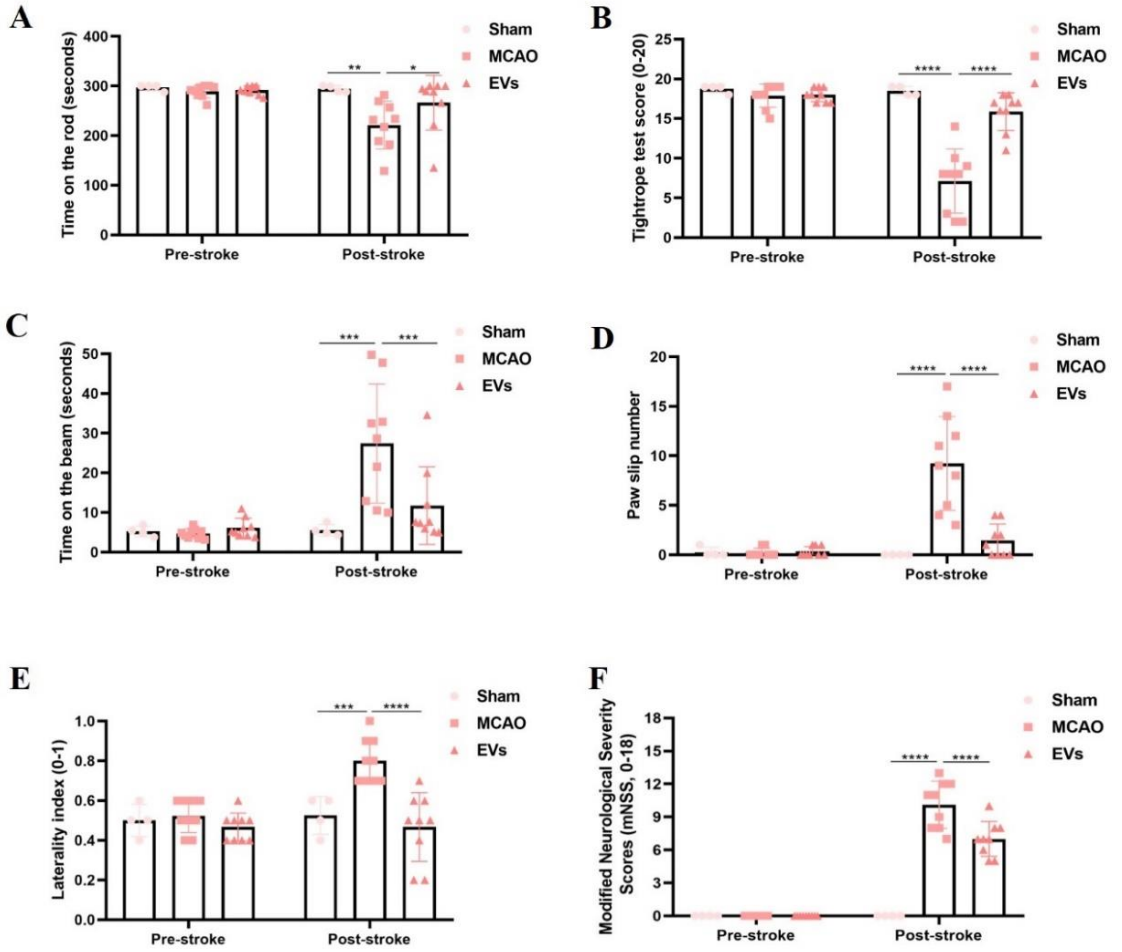

Figure 22: EV delivery protects against ischemia-induced postischemic motor coordination impairment. The rotarod test (A), the tightrope test (B), the balance beam test (C), the paw slips recording (D) the corner turn test (E), and the modified neurological severity scores (F) were tested on the day 1 before stroke and day 7 after stroke. *p < 0.05, **p < 0.01, ***p < 0.001, ****p < 0.0001; MCAO, middle cerebral artery occlusion; EVs, extracellular vesicles.

4. Discussion

The survival of neurons and glial cells is affected by the occlusion of a cerebral artery. Brain neurons are the most vulnerable of these different cells, and the healing of destroyed neurological functions requires neuronal viability, structural connectivity, and functional responses (Hermann et al. 2022). The successful restoration of glial functions, on the other hand, is critical to neurological recovery following a stroke (Hermann et al. 2022). Neurons and glial cells interact closely during the remodeling of brain tissue, laying the groundwork for effective neurological recovery (Hermann et al. 2022). Experimental stroke studies demonstrated that EVs from microglia could boost ischemic brain tissue survival (Li et al. 2022). The underlying modulation of the specific pathophysiological aspects of such EV-induced beneficial effects under stroke conditions, however, remains elusive. Employing both an in vitro and an in vivo stroke model, the current work aimed to identify a new mode of action by which EVs derived from hypoxic microglia mediate poststroke neuroprotection and neurological recovery. The aim of this study was to assess the influence of EVs produced by microglia after OGD on ischemia-mediated astrogliosis, AQP4 depolarization and neuroinflammation.

4.1. Cell source, identification of cells, and EV isolation.

To isolate microglial EVs, the BV2 cell line and primary microglia are the two cell sources available. Since often do not represent the 'real' situation in vivo, primary microglia were chosen for this study to be closer to the in vivo situation. Additionally, our team has long-time experience in isolating and cultivating mouse microglia (Zhang et al. 2021a). Concerning the purpose of studying the effect of EVs on the AQP4 level, primary astrocytes and the astrocyte cell line C8D1A are the two cell sources available. Again, primary astrocytes are the optimal selection because AQP4 is frequently expressed in primary astrocytes (Tang et al. 2022; Zhu et al. 2022). More importantly, the isolation of primary microglia and primary astrocytes can be done at the same time (Lanfranco et al. 2021; Long et al. 2020). EVs are cellular secretions that contain proteins, DNA, RNA, and lipids, showing the characteristics of the donor cell and its state of physiology (Zamani et al. 2019). The primary membrane-bound and cytosolic proteins incorporated in EVs include several types: (I) the tetraspanin family members, such as CD9, CD63, and CD81; (II) the endosomal sorting complex required for transport proteins, such as Alix and TSG101; (III) and other molecules, namely integrins and flotillins (Garcia et al. 2015; Zhang et al. 2019). Western blotting was used in this investigation to identify numerous common EV markers, including TSG101, CD9, Alix,

CD81, and CD63, in the vesicular fractions that were collected. Normally, EVs present a spheroid shape in solution, however, during isolation, they exhibit a bi-concave or cup-shaped due to artificial drying. In our experiments, we employed a TEM, demonstrating a typical EV morphology. NTA meantime was adopted to quantify and determine the magnitude of these vesicles (Wei et al. 2019). It was discovered that the size range of these EVs, which are typical of exosomes and microvesicles alike, was between 50 and 200 nm. With the growing knowledge about EV, the potential therapeutic role has been steadily explored. Reproducible separation and enrichment of EVs are therefore mandatory to evaluate their biological value. Nonetheless, EVs are different in size, cargo, function, and source, which makes separation strategies difficult (Kalluri and LeBleu 2020). Due to its great processing capacity, ultracentrifugation has long been considered the "gold standard" for EV isolation; nonetheless, it has been noted that EV samples using this isolation method include significant amounts of protein and lipoprotein contamination (Hermann et al. 2022). The contamination further compromises their quantification and function. Since it is impractical to use a single approach to separate EVs from a range of sample sources, efforts should be made to investigate the creation of novel devices and techniques. As previously mentioned, the PEG precipitation method was used in the current work to extract EVs (Théry et al. 2018).

4.2. Effect of EV administration on neuroinflammation.

The CNS innate and peripheral immune responses, as well as inflammation, play important regulatory functions throughout the entire pathogenesis of stroke. Following a stroke, several inflammatory mediators disseminate throughout the cerebrospinal fluid or intercellular fluid due to the impairment of microvascular endothelial cells across the entire brain and the rupture of the blood-brain barrier (Malone et al. 2019). Meanwhile, activated glial cells begin to appear in the infarct area and surrounding tissue, accompanied by the infiltration of many peripheral immune cells, gradually forming a whole brain inflammatory environment (Shi et al. 2019). The inflammatory response has two sides: on the one hand, activated inflammatory cells can phagocytose dead cells or debris to facilitate tissue repair; on the other hand, an over-activated inflammatory response will worsen neuronal injury (Lambertsen et al. 2019). Thus, the inflammatory response has become a wide target for the treatment of ischemic stroke.

Recent research work showed that EVs can control tissue healing and inflammation under preclinical ischemic stroke settings. For instance, Toll-like receptor 4 (TLR4) on

inflammatory cells is activated after an ischemic stroke, causing inflammation and subsequent neuronal damage. By blocking TLR4, the miR-542-3p delivered by MSC-exosomes can reduce glial cell inflammatory response and the death of neurons (Cai et al. 2021). Furthermore, according to Yang and Chen (Yang and Chen 2022), exosomes containing the long noncoding RNA ZFAS1 reduced oxidative stress and neuroinflammation in ischemic stroke. Microglia are the primary component of the innate immune system in CNS and are thought to be the first non-nerve cells to respond to ischemic stroke (Xin et al. 2021). Upon a stroke, the inflammatory response is triggered immediately, and microglia are activated and can be divided into two types: M1 (pro-inflammatory) and M2 (anti-inflammatory) (Han et al. 2021). In order to prevent brain damage following a stroke, the modulation of microglial polarization can be employed as a therapeutic target. For example, by altering the M1/M2 phenotypes of microglia, MSC-derived EVs reduce the neuroinflammation induced by cerebral ischemia-reperfusion injury (Liu et al. 2021). Likewise, through controlling microglial polarization, Zheng et al.(Zheng et al. 2019) demonstrated that EVs from LPS-activated macrophages support poststroke repair of neuronal function.

It has been demonstrated that microglia encourage cell-cell interaction in treating cerebral ischemia via many approaches, most reported via the secretion of EVs (Li et al. 2022). Additionally, microglia of different activation states may represent different EV cargos and thereby yield different functions. For instance, neuronal autophagy, apoptosis, and glial scar formation can all be inhibited by M2 microglia-derived EVs, which then enhance neuroprotection (Li et al. 2022). Likewise, Tian et al. demonstrated that IL-4-treated BV2 microglia cells can inhibit ischemic stroke injury by promoting angiogenesis via EVs release (Tian et al. 2019). Of note, in our research group, in a mouse model of ischemic stroke, we have previously shown that EVs produced from hypoxic microglia stimulate angiogenesis and prevent cell apoptosis via the TGF-β signalling (Zhang et al. 2021a). Therefore, given the anti-inflammatory function of M2 microglia and the therapeutic effect of EVs from hypoxic microglia on neuroprotection, it is reasonable to assume such EVs may regulate the pathogenesis of neuroinflammation as well. Therefore, we hypothesize that OGD-microglia-derived EVs show neuroprotective effects by suppressing neuroinflammation. First, we investigated how these EVs affected the polarization of the microglia. The results show that M2-type microglia marker levels were elevated by such EVs. The levels of M1-type microglia marker levels were decreased in the EV treatment group. As the above data show, such EVs have the potential to repress M1 microglia polarization and promote M2 microglia polarization. Besides, the treatment with EVs shows a similar observation in terms of inflammation in hypoxic astrocyte. Similarly, Song et al. indicated that that EVs from M2

microglia treated with treated with IL-4 inhibited the inflammation and immune responses in the poststroke mice (Song et al. 2019). Taken together, the present work indicates EVs from OGD-preconditioned microglia can inhibit neuroinflammation.

EVs contain a variety of molecular cargo, e.g., RNAs, DNAs, lipids, and metabolites, which partly exhibit the transcriptomes of corresponding donor cells. It is reasonable to think that such EVs with a similar profile to the M2 microglia are involved in regulating inflammation. Cell-based therapies using M2 microglia, however, do not only rely on the protective abilities of these released EVs but also on their protective cargos, such as TGF-β1 (Zhang et al. 2021a). The TGF-β family of cytokines is ubiquitous, multifunctional, and important for cell survival. They are the key players across a range of cellular processes, which are important for the growth and development of tissue and organs (Clark and Coker 1998; Fabregat et al. 2016). TGF-β1, one of the three TGF-β isoforms (the others being TGF-β2 and TGF-β3), is regarded as an anti-inflammatory agent (Lodyga and Hinz 2020). Researchers have revealed the anti-inflammatory effect of TGF-β1 during progressive kidney injury (Loboda et al. 2016). In a model of obstructive kidney disease, severe inflammation, involving vast T cell and macrophage infiltration, IL-1β and TNF-α levels were significantly boosted, however, the such inflammatory response was reversed in TGF-β1 overexpression mice (Wang et al. 2005). Additionally, TGF-β1 knockout causes several inflammatory disorders in various tissues, herein, the heart and lungs are mostly affected (Yaswen et al. 1996). In this study, the expression of TGF-1 was considerably increased in microglia after OGD. A boosted TGF-β1 level was further related to a higher level of cell viability. In addition, a higher level of microglial EV-TGF-β1 has the potential to promote M2-type microglia polarization, while EVs derived from hypoxic TGF-β1 knockdown microglia report a lower level of M2-type microglia polarization compared to the group of EVs derived from hypoxic microglia. Islam and colleagues (Islam et al. 2018) indicated that abundant TGF-β1 expression in the poststroke brain had significant anti-inflammatory effects on microglia via suppressing endogenous Toll-like receptor ligand pathway. Altogether, in this study, mechanistically, one can suggest an anti-inflammatory effect of EVs derived from OGD microglia via the TGF-β1 pathway. However, information regarding this phenomenon is scarce, and more evidence-based information is needed in this respect.

4.3. Effects of EV administration on astrogliosis and AQP4 depolarization.

One of the most prevalent types of CNS cells, astrocytes, change to a reactive phenotype during a stroke syndrome known as reactive astrogliosis, which is characterized by the up-regulation of GFAP and cellular hypertrophy (Pekny Milos and Pekna 2014; Sofroniew 2009). Thereafter, these reactive astrocytes move to the infarct and peri-infarct region, followed by proliferation in the peri-infarct region, leading to glial scar formation. Reactive astrogliosis can form a dense meshwork and finally result in a barrier for neurite outgrowth, thereby suppressing poststroke neurological function recovery (Cregg et al. 2014; Zhang et al. 2018). Numerous studies have uncovered that the inhibition of glial scar formation and reactive astrogliosis can help stroke mice regain neurological function. For instance, Dong and co-workers (Dong et al. 2021) demonstrated that salidroside could inhibit reactive astrogliosis, reduce glial scar formation, and promote long-term neurological functional recovery. Likewise, Zhong et al. found that saffron, a dry stigma of the plant Crocus sativus L., exhibited a neuroprotective effect on late ischemic stroke, leading to a reduction of astrogliosis and glial scar formation (Zhong et al. 2020). Additionally, evidence suggests that astrocytes and microglia work together to generate glial scars (Zhong et al. 2020), however, only few researchers have investigated how microglia modulate reactive astrogliosis and the impact of EVs derived from OGD microglia in this process (Li et al. 2021). Therefore, we aimed to estimate the effect of EVs derived from OGD microglia on the regulation of astrogliosis. We first analyzed the dynamic astrogliosis after ischemic stroke, revealing the higher levels of astrocyte marker GFAP at many time points in the peri-infarct cortex. EVs derived from hypoxic microglia attenuated astrogliosis in several regions of the peri-infarct cortex. In addition to the EVs from hypoxic microglia, exosomes from M2 BV2 cells induced by IL-4 treatment have the potential to repress glial scar formation in a preclinical poststroke model (Li et al. 2021). Taken together, microglia can suppress glial scar formation via EVs release, thereby promoting poststroke neurological function recovery.

Iliff et al. have recently suggested a network of perivascular spaces that promote the movement of cerebrospinal fluid into the brain and clearance of interstitial solutes from the brain parenchyma (Iliff and Nedergaard 2013). The exchange of cerebrospinal fluid with interstitial fluid is regarded to be promoted via the AQP4 water channels on astrocytic endfeet (Holter et al. 2017; Iliff et al. 2012; Xie et al. 2013). AQP4 knock-out mice showed an approximately 70% decrease in cerebrospinal fluid influx and an about 55% decrease in parenchymal solute clearance (Iliff et al. 2012; Mestre et al. 2018). Thus, an appropriate

expression pattern of AQP4 localized to perivascular astrocytic endfeet (called AQP4 polarization) is required for efficient waste clearance (Mestre et al. 2018; Zeppenfeld et al. 2017). Interestingly, AQP4 polarization reduces with age (Mestre et al. 2018; Zeppenfeld et al. 2017). In addition, it was reported recently that AQP4 polarization disappeared after stroke (Sun et al. 2022; Zhu et al. 2022), revealing that impaired AQP4 polarization may be a novel stroke treatment target. Sun et al. indicated that using TGN-020, an AQP4 inhibitor, promoted neurological function recovery by reducing brain edema, reactive astrogliosis, and AQP4 depolarization after stroke (Sun et al. 2022). The EVs from OGD microglia were injected into the MCAO mouse to assess the AQP4 polarity in the day 7 peri-infarct cortex. The results demonstrated that EVs from OGD microglia had a supportive effect on the AQP4 polarity in all regions of the day 7 peri-infarct cortex. Importantly, after stroke and other CNS disorders condition, reactive astrogliosis is invariably accompanied by the appearance of AQP4 depolarization in the same region. Sun et al. showed that AQP4 depolarization was related positively to reactive astrogliosis in the same region, suggesting that reactive astrogliosis might be involved in AQP4 depolarization (Sun et al. 2022). In addition, the strong connection between reactive astrogliosis and AQP4 depolarization was demonstrated in multiple preclinical CNS disease models, such as traumatic brain injury and multiple microinfarcts (He et al. 2020; Liu et al. 2015). Some researchers insist the appearance of AQP4 depolarization is a primary characteristic of astrogliosis instead of a pathological consequence of impaired astrocytic endfeet (Liddelow and Barres 2017; Smith et al. 2019). We, therefore, think the reduced astrogliosis after EV treatment might protect AQP4 from depolarization after stroke.

During stroke conditions, although the AQP4 level increases, an AQP4 depolarization appears, indicating AQP4 will change location from the perivascular region to the whole membrane of the astrocyte. Consequently, interstitial protein and interstitial fluid protein clearing from the brain via perivenous space will be delayed. Such AQP4 polarization affects the clearance of brain metabolites (Boland et al. 2018), involving amyloid β in Alzheimer's disease (Mader and Brimberg 2019). Besides, during inflammation, the cerebrospinal fluid flow would be blocked, influencing the clearance of proteins due to massive immune cell infiltration in perivascular spaces (Mogensen et al. 2021). Of note, peripheral inflammatory cytokines may be transported to the brain parenchyma through the perivascular space, bypassing the arachnoid mater (Troili et al. 2020). Furthermore, the brain of AQP4 knockout mice displayed increased microglial activation and neutrophil infiltration after stroke compared to the brain of control mice (Shi et al. 2012). Therefore, the breakdown of these barriers induces neuroinflammation as the normal response in the preclinical stages of CNS

diseases, and the recovery of AQP4 polarization contributes to the inhibition of neuroinflammation.

4.4. EVs administration promotes neurological function recovery

According to the WHO, stroke was the leading cause of death and years of adjusted life (Xiong et al. 2022). Stroke leads to long-term sensory, cognitive and visual impairment, and reduced motor behaviour, thus decreasing neurological functions (Katzan et al. 2018). Poststroke destroyed motor function is the most suggested complication, therein, 80% of cases approximately develop hemiplegia (Kim et al. 2020). More importantly, 50% of these symptoms will last forever, significantly influencing patients' daily life (Kim et al. 2020). Undoubtedly, hemiplegia is the main cause of lasting poststroke disability. Thus, improving poststroke neurological function recovery is essential. Although effective rehabilitation training can accelerate motor function in hemiplegic limbs, thereby promoting poststroke neurological function recovery, it is limited. Currently, analysis of behavioral test results shows that mice receiving EV injections perform better in behavioural tests. These neurological improvements were long-lasting (Haupt et al. 2021; Vu et al. 2014). Similarly, the present study also indicates that EV administration is associated with improved poststroke motor coordination. Down-regulated AQP4 polarization-associated poststroke edema plays a crucial role in the development of stroke and prevents improvement from a stroke. Sun et al. indicated that TGN-020 could improve neurological function recovery by postischemic repressing brain edema, peri-infarct astrogliosis, and AQP4 depolarization (Sun et al. 2022). As such, our data also showed a similar observation via delivering the hypoxic microglial EVs.

4.5. Limitations

The current study does have certain limitations. This study demonstrates that EVs secreted by OGD microglia improve AQP4 polarization and inhibit astrogliosis and neuroinflammation after stroke. However, the underlying molecular mechanisms need to be further elucidated. Although previous studies of our group pointed out that TGF-β is the main bearer of EVs from hypoxic microglia, this study did not investigate the role of TGF-β. Further research is still needed to clarify this issue. Furthermore, based on previous studies, AQP4 polarization may have a regulatory effect on inflammation, however, this study does not employ specific AQP4 knockout mice to evaluate its influence on inflammation under

stroke conditions. We set up an in vitro co-culture between primary astrocytes and microglia to demonstrate whether AQP4 participates in the astrocyte–microglia neuroinflammation communication or not. We used astrocytes of different states because their AQP4 expression levels were not consistent, however, these astrocytes likely had changes in other components besides AQP4, therefore, the use of AQP4 deficient astrocytes appears more suitable in future studies.

5. Summary

Stroke is among the primary causes of mortality and disability in the world. After a stroke, neurons in the ischemic region die irreversibly, causing neurological impairments. EVs are crucial for cell-to-cell communication by delivering cargo to recipient cells, also in the brain. In particular, recent studies have recommended microglial EVs as a novel treatment option for stroke. The attention of such treatment has been directed toward glial and neurological function recovery. The present study gives a novel notion to poststroke-specific AQP4 depolarization, astrogliosis, and inflammation. In vitro, an OGD condition promoted M2 microglial polarization, and an increased concentration of such EVs in OGD microglia was related to a higher expression of the M2 microglial polarization markers and a lower level of the M1 microglial polarization markers. Moreover, EVs also attenuated the upregulation of AQP4 clustering and pro-inflammatory cytokines in astrocytes challenged by OGD. However, an alteration of the AQP4 expression in astrocytes was not involved in modulating astrocyte-to-microglia inflammation communication. In vivo, EV treatment augments postischemic cerebral perfusion and motor coordination impairment and diminished postischemic brain edema. EVs in the meantime reduce peri-infarct AQP4 depolarization, astrogliosis, and inflammation. Therefore, the results suggest, for the first time, that hypoxic microglia may participate in protecting against stroke-induced brain damage by diminishing postischemic inflammation, astrogliosis and AQP4 depolarization. This investigation may represent a novel perspective on stroke treatment.

6. References

Assentoft M, Larsen BR, MacAulay N (2015): Regulation and Function of AQP4 in the Central Nervous System. Neurochem Res 40, 2615-2627

Badaut J, Fukuda AM, Jullienne A, Petry KG (2014): Aquaporin and brain diseases. Biochim Biophys Acta 1840, 1554-1565

Balkaya M, Kröber JM, Rex A, Endres M (2013): Assessing post-stroke behavior in mouse models of focal ischemia. J Cereb Blood Flow Metab 33, 330-338

Ballabh P, Braun A, Nedergaard M (2004): The blood-brain barrier: an overview: structure, regulation, and clinical implications. Neurobiol Dis 16, 1-13

Barthels D, Das H (2020): Current advances in ischemic stroke research and therapies. Biochim Biophys Acta Mol Basis Dis 1866, 165260

Battistelli M, Falcieri E (2020): Apoptotic bodies: particular extracellular vesicles involved in intercellular communication. Biology 9, 21

Benfenati V, Nicchia GP, Svelto M, Rapisarda C, Frigeri A, Ferroni S (2007): Functional down-regulation of volume-regulated anion channels in AQP4 knockdown cultured rat cortical astrocytes. J Neurochem 100, 87-104

Benjamin EJ, Virani SS, Callaway CW, Chamberlain AM, Chang AR, Cheng S, Chiuve SE, Cushman M, Delling FN, Deo R (2018): Heart disease and stroke statistics—2018 update: a report from the American Heart Association. Circulation 137, e67-e492

Boehme AK, Esenwa C, Elkind MS (2017): Stroke Risk Factors, Genetics, and Prevention. Circ Res 120, 472-495

Boland B, Yu WH, Corti O, Mollereau B, Henriques A, Bezard E, Pastores GM, Rubinsztein DC, Nixon RA, Duchen MR, et al. (2018): Promoting the clearance of neurotoxic proteins in neurodegenerative disorders of ageing. Nat Rev Drug Discov 17, 660-688

Butovsky O, Jedrychowski MP, Moore CS, Cialic R, Lanser AJ, Gabriely G, Koeglsperger T, Dake B, Wu PM, Doykan CE (2014): Identification of a unique TGF-β–dependent molecular and functional signature in microglia. Nat Neurosci 17, 131-143

Cai G, Cai G, Zhou H, Zhuang Z, Liu K, Pei S, Wang Y, Wang H, Wang X, Xu S, et al. (2021): Mesenchymal stem cell-derived exosome miR-542-3p suppresses inflammation and prevents cerebral infarction. Stem Cell Res Ther 12, 2

Campbell BC, Mitchell PJ, Kleinig TJ, Dewey HM, Churilov L, Yassi N, Yan B, Dowling RJ, Parsons MW, Oxley TJ, et al. (2015): Endovascular therapy for ischemic stroke with perfusion-imaging selection. N Engl J Med 372, 1009-1018

Carter RJ, Lione LA, Humby T, Mangiarini L, Mahal A, Bates GP, Dunnett SB, Morton AJ (1999): Characterization of progressive motor deficits in mice transgenic for the human Huntington's disease mutation. J Neurosci 19, 3248-3257

Chhor V, Le Charpentier T, Lebon S, Oré MV, Celador IL, Josserand J, Degos V, Jacotot E, Hagberg H, Sävman K, et al. (2013): Characterization of phenotype markers and neuronotoxic potential of polarised primary microglia in vitro. Brain Behav Immun 32, 70-85

Choudhury GR, Ding S (2016): Reactive astrocytes and therapeutic potential in focal ischemic stroke. Neurobiol Dis 85, 234-244

Clark DA, Coker R (1998): Transforming growth factor-beta (TGF-beta). Int J Biochem Cell Biol 30, 293-298

Clasadonte J, Dong J, Hines DJ, Haydon PG (2013): Astrocyte control of synaptic NMDA receptors contributes to the progressive development of temporal lobe epilepsy. Proc Natl Acad Sci U S A 110, 17540-17545

Clément T, Rodriguez‐Grande B, Badaut J (2020): Aquaporins in brain edema. J Neurosci Res 98, 9-18

Colombo E, Farina C (2016): Astrocytes: Key Regulators of Neuroinflammation. Trends Immunol 37, 608-620

Cregg JM, DePaul MA, Filous AR, Lang BT, Tran A, Silver J (2014): Functional regeneration beyond the glial scar. Exp Neurol 253, 197-207

Dai W, Yan J, Chen G, Hu G, Zhou X, Zeng X (2018): AQP4‐knockout alleviates the lipopolysaccharide‐induced inflammatory response in astrocytes via SPHK1/MAPK/AKT signaling. Int J Mol Med 42, 1716-1722

Dasdelen D, Mogulkoc R, Baltaci AK (2020): Aquaporins and Roles in Brain Health and Brain Injury. Mini Rev Med Chem 20, 498-512

DeGraba TJ (1998): The role of inflammation after acute stroke: utility of pursuing anti-adhesion molecule therapy. Neurology 51, S62-68

Diener HC (2000): Stroke prevention: anti-platelet and anti-thrombolytic therapy. Neurol Clin 18, 343-355

Dong C, Wen S, Zhao S, Sun S, Zhao S, Dong W, Han P, Chen Q, Gong T, Chen W, et al. (2021): Salidroside Inhibits Reactive Astrogliosis and Glial Scar Formation in Late Cerebral Ischemia via the Akt/GSK-3β Pathway. Neurochem Res 46, 755-769

Doyle LM, Wang MZ (2019): Overview of extracellular vesicles, their origin, composition, purpose, and methods for exosome isolation and analysis. Cells 8, 727

Fabregat I, Moreno-Càceres J, Sánchez A, Dooley S, Dewidar B, Giannelli G, Ten Dijke P (2016): TGF-β signalling and liver disease. FEBS J 283, 2219-2232

Fann DY, Lee SY, Manzanero S, Chunduri P, Sobey CG, Arumugam TV (2013): Pathogenesis of acute stroke and the role of inflammasomes. Ageing Res Rev 12, 941-966

Filchenko I, Blochet C, Buscemi L, Price M, Badaut J, Hirt L (2020): Caveolin-1 Regulates Perivascular Aquaporin-4 Expression After Cerebral Ischemia. Front Cell Dev Biol 8, 371

Filiano AJ, Gadani SP, Kipnis J (2015): Interactions of innate and adaptive immunity in brain development and function. Brain Res 1617, 18-27

Fischer R, Wajant H, Kontermann R, Pfizenmaier K, Maier O (2014): Astrocyte-specific activation of TNFR2 promotes oligodendrocyte maturation by secretion of leukemia inhibitory factor. Glia 62, 272-283

Gao C, Qian Y, Huang J, Wang D, Su W, Wang P, Guo L, Quan W, An S, Zhang J (2017): A three-day consecutive fingolimod administration improves neurological functions and modulates multiple immune responses of CCI mice. Mol Neurobiol 54, 8348-8360

Garcia NA, Ontoria-Oviedo I, González-King H, Diez-Juan A, Sepúlveda P (2015): Glucose starvation in cardiomyocytes enhances exosome secretion and promotes angiogenesis in endothelial cells. PloS One 10, e0138849

Gil-Garcia CA, Flores-Alvarez E, Cebrian-Garcia R, Mendoza-Lopez AC, Gonzalez-Hermosillo LM, Garcia-Blanco MD, Roldan-Valadez E (2022): Essential Topics About the Imaging Diagnosis and Treatment of Hemorrhagic Stroke: A Comprehensive Review of the 2022 AHA Guidelines. Curr Probl Cardiol 47, 101328

References

Goyal M, Demchuk AM, Menon BK, Eesa M, Rempel JL, Thornton J, Roy D, Jovin TG, Willinsky RA, Sapkota BL, et al. (2015): Randomized assessment of rapid endovascular treatment of ischemic stroke. N Engl J Med 372, 1019-1030

Gurung S, Perocheau D, Touramanidou L, Baruteau J (2021): The exosome journey: from biogenesis to uptake and intracellular signalling. Cell Commun Signal 19, 47

Hackett ML, Anderson CS (2000): Health outcomes 1 year after subarachnoid hemorrhage: an international population-based study. Neurology 55, 658-662

Han B, Jiang W, Cui P, Zheng K, Dang C, Wang J, Li H, Chen L, Zhang R, Wang QM, et al. (2021): Microglial PGC-1α protects against ischemic brain injury by suppressing neuroinflammation. Genome Med 13, 47

Haupt M, Zheng X, Kuang Y, Lieschke S, Janssen L, Bosche B, Jin F, Hein K, Kilic E, Venkataramani V, et al. (2021): Lithium modulates miR-1906 levels of mesenchymal stem cell-derived extracellular vesicles contributing to poststroke neuroprotection by toll-like receptor 4 regulation. Stem Cells Transl Med 10, 357-373

He XF, Li G, Li LL, Li MY, Liang FY, Chen X, Hu XQ (2020): Overexpression of Slit2 decreases neuronal excitotoxicity, accelerates glymphatic clearance, and improves cognition in a multiple microinfarcts model. Mol Brain 13, 135

Hellings WE, Peeters W, Moll FL, Pasterkamp G (2007): From vulnerable plaque to vulnerable patient: the search for biomarkers of plaque destabilization. Trends Cardiovasc Med 17, 162-171

Hermann DM, Xin W, Bähr M, Giebel B, Doeppner TR (2022): Emerging roles of extracellular vesicle-associated non-coding RNAs in hypoxia: Insights from cancer, myocardial infarction and ischemic stroke. Theranostics 12, 5776-5802

Holter KE, Kehlet B, Devor A, Sejnowski TJ, Dale AM, Omholt SW, Ottersen OP, Nagelhus EA, Mardal K-A, Pettersen KH (2017): Interstitial solute transport in 3D reconstructed neuropil occurs by diffusion rather than bulk flow. Proc Natl Acad Sci U S A 114, 9894-9899

Hou C, Li J, Wang B, Liu Q, Zhao Y, Zhang H, Wang W, Ren W, Cui X, Yang X (2022): Dynamic Evolution of the Glymphatic System at the Early Stages of Subarachnoid Hemorrhage. Front Neurol 13, 924080

Huang L, Wu ZB, Zhuge Q, Zheng W, Shao B, Wang B, Sun F, Jin K (2014): Glial scar formation occurs in the human brain after ischemic stroke. Int J Med Sci 11, 344-348

References

Hung CC, Lin CH, Chang H, Wang CY, Lin SH, Hsu PC, Sun YY, Lin TN, Shie FS, Kao LS, et al. (2016): Astrocytic GAP43 Induced by the TLR4/NF-κB/STAT3 Axis Attenuates Astrogliosis-Mediated Microglial Activation and Neurotoxicity. J Neurosci 36, 2027-2043

Ikeshima-Kataoka H (2016): Neuroimmunological Implications of AQP4 in Astrocytes. Int J Mol Sci 17

Iliff J, Wang M, Liao Y, Plogg B, Peng W, Gundersen G, Benveniste H, Vates G, Deane R, Goldman S: A paravascular pathway facilitates CSF flow through the brain parenchyma and the clearance of interstitial solutes, including amyloid β. Sci Transl Med 4, 147ra111 (2012). hrsg. 2012

Iliff JJ, Nedergaard M (2013): Is there a cerebral lymphatic system? Stroke 44, S93-95

Islam A, Choudhury ME, Kigami Y, Utsunomiya R, Matsumoto S, Watanabe H, Kumon Y, Kunieda T, Yano H, Tanaka J (2018): Sustained anti-inflammatory effects of TGF-β1 on microglia/macrophages. Biochim Biophys Acta Mol Basis Dis 1864, 721-734

Jeppesen D, Fenix A, Franklin J, Higginbotham J, Zhang Q, Zimmerman L, Liebler D, Ping J, Liu Q, Evans R, et al. (2019): Reassessment of Exosome Composition. Cell 177, 428-445.e418

Ji C, Yu X, Xu W, Lenahan C, Tu S, Shao A (2021): The role of glymphatic system in the cerebral edema formation after ischemic stroke. Exp Neurol 340, 113685

Jin Q, Cheng J, Liu Y, Wu J, Wang X, Wei S, Zhou X, Qin Z, Jia J, Zhen X (2014): Improvement of functional recovery by chronic metformin treatment is associated with enhanced alternative activation of microglia/macrophages and increased angiogenesis and neurogenesis following experimental stroke. Brain Behav Immun 40, 131-142

Jin R, Liu L, Zhang S, Nanda A, Li G (2013): Role of inflammation and its mediators in acute ischemic stroke. J Cardiovasc Transl Res 6, 834-851

Kalluri R, LeBleu VS (2020): The biology, function, and biomedical applications of exosomes. Science 367, eaau6977

Kapil N, Datta YH, Alakbarova N, Bershad E, Selim M, Liebeskind DS, Bachour O, Rao GHR, Divani AA (2017): Antiplatelet and Anticoagulant Therapies for Prevention of Ischemic Stroke. Clin. Appl. Thromb Hemost 23, 301-318

Karch J, Molkentin JD (2015): Regulated necrotic cell death: the passive aggressive side of Bax and Bak. Circ Res 116, 1800-1809

Kario K, Ishikawa J, Pickering TG, Hoshide S, Eguchi K, Morinari M, Hoshide Y, Kuroda T, Shimada K (2006): Morning hypertension: the strongest independent risk factor for stroke in elderly hypertensive patients. Hypertens Res 29, 581-587

Katzan IL, Schuster A, Newey C, Uchino K, Lapin B (2018): Patient-reported outcomes across cerebrovascular event types: More similar than different. Neurology 91, e2182-e2191

Kim J, Thayabaranathan T, Donnan GA, Howard G, Howard VJ, Rothwell PM, Feigin V, Norrving B, Owolabi M, Pandian J (2020): Global stroke statistics 2019. Int J Stroke 15, 819-838

Klegerman ME (2017): Translational initiatives in thrombolytic therapy. Front Med 11, 1-19

Koyama Y (2014): Signaling molecules regulating phenotypic conversions of astrocytes and glial scar formation in damaged nerve tissues. Neurochem Int 78, 35-42

Kress BT, Iliff JJ, Xia M, Wang M, Wei HS, Zeppenfeld D, Xie L, Kang H, Xu Q, Liew JA, et al. (2014): Impairment of paravascular clearance pathways in the aging brain. Ann Neurol 76, 845-861

Kruse E, Uehlein N, Kaldenhoff R (2006): The aquaporins. Genome Biol 7, 206

Kuang Y, Zheng X, Zhang L, Ai X, Venkataramani V, Kilic E, Hermann DM, Majid A, Bähr M, Doeppner TR (2020): Adipose-derived mesenchymal stem cells reduce autophagy in stroke mice by extracellular vesicle transfer of miR-25. J Extracell Vesicles 10, e12024

Lambertsen KL, Finsen B, Clausen BH (2019): Post-stroke inflammation-target or tool for therapy? Acta Neuropathol 137, 693-714

Lan X, Han X, Li Q, Yang QW, Wang J (2017): Modulators of microglial activation and polarization after intracerebral haemorrhage. Nat Rev Neurol 13, 420-433

Lanfranco MF, Sepulveda J, Kopetsky G, Rebeck GW (2021): Expression and secretion of apoE isoforms in astrocytes and microglia during inflammation. Glia 69, 1478-1493

Li F, Kang X, Xin W, Li X (2022): The Emerging Role of Extracellular Vesicle Derived From Neurons/Neurogliocytes in Central Nervous System Diseases: Novel Insights Into Ischemic Stroke. Front Pharmacol 13, 890698

Li G, Xiao L, Qin H, Zhuang Q, Zhang W, Liu L, Di C, Zhang Y (2020): Exosomes-carried microRNA-26b-5p regulates microglia M1 polarization after cerebral ischemia/reperfusion. Cell Cycle 19, 1022-1035

Li Z, Song Y, He T, Wen R, Li Y, Chen T, Huang S, Wang Y, Tang Y, Shen F, et al. (2021): M2 microglial small extracellular vesicles reduce glial scar formation via the miR-124/STAT3 pathway after ischemic stroke in mice. Theranostics 11, 1232-1248

Lian H, Roy E, Zheng H (2016): Protocol for primary microglial culture preparation. Bio Protoc 6, e1989-e1989

Liddelow SA, Barres BA (2017): Reactive Astrocytes: Production, Function, and Therapeutic Potential. Immunity 46, 957-967

Lilja-Cyron A, Eskesen V, Hansen K, Kondziella D, Kelsen J (2016): [Acute surgical treatment of malignant stroke]. Ugeskr Laeger 178

Linnerbauer M, Rothhammer V (2020): Protective Functions of Reactive Astrocytes Following Central Nervous System Insult. Front Immunol 11, 573256

Liu H, Qiu G, Zhuo F, Yu W, Sun S, Li F, Yang M (2015): Lost Polarization of Aquaporin4 and Dystroglycan in the Core Lesion after Traumatic Brain Injury Suggests Functional Divergence in Evolution. Biomed Res Int 2015, 471631

Liu X, Zhang M, Liu H, Zhu R, He H, Zhou Y, Zhang Y, Li C, Liang D, Zeng Q, et al. (2021): Bone marrow mesenchymal stem cell-derived exosomes attenuate cerebral ischemia-reperfusion injury-induced neuroinflammation and pyroptosis by modulating microglia M1/M2 phenotypes. Exp Neurol 341, 113700

Liu Y, Li Y-P, Xiao L-M, Chen L-K, Zheng S-Y, Zeng E-M, Xu C-H (2021): Extracellular vesicles derived from M2 microglia reduce ischemic brain injury through microRNA-135a-5p/TXNIP/NLRP3 axis. Lab Invest 101, 837-850

Loboda A, Sobczak M, Jozkowicz A, Dulak J (2016): TGF-β1/Smads and miR-21 in Renal Fibrosis and Inflammation. Mediators Inflamm 2016, 8319283

Lodyga M, Hinz B (2020): TGF-β1 - A truly transforming growth factor in fibrosis and immunity. Semin Cell Dev Biol 101, 123-139

Long X, Yao X, Jiang Q, Yang Y, He X, Tian W, Zhao K, Zhang H (2020): Astrocyte-derived exosomes enriched with miR-873a-5p inhibit neuroinflammation via microglia phenotype modulation after traumatic brain injury. J Neuroinflammation 17, 89

Ma Y, Wang J, Wang Y, Yang GY (2017): The biphasic function of microglia in ischemic stroke. Prog Neurobiol 157, 247-272

MacDonald JF, Xiong ZG, Jackson MF (2006): Paradox of Ca2+ signaling, cell death and stroke. Trends Neurosci 29, 75-81

Mader S, Brimberg L (2019): Aquaporin-4 Water Channel in the Brain and Its Implication for Health and Disease. Cells 8, 90

Malik P, Anwar A, Patel R, Patel U (2021): Expansion of the dimensions in the current management of acute ischemic stroke. J Neurol 268, 3185-3202

Malone K, Amu S, Moore AC, Waeber C (2019): The immune system and stroke: from current targets to future therapy. Immunol Cell Biol 97, 5-16

Manley GT, Binder DK, Papadopoulos MC, Verkman AS (2004): New insights into water transport and edema in the central nervous system from phenotype analysis of aquaporin-4 null mice. Neuroscience 129, 983-991

Manley GT, Fujimura M, Ma T, Noshita N, Filiz F, Bollen AW, Chan P, Verkman AS (2000): Aquaporin-4 deletion in mice reduces brain edema after acute water intoxication and ischemic stroke. Nat Med 6, 159-163

Mendelson SJ, Prabhakaran S (2021): Diagnosis and Management of Transient Ischemic Attack and Acute Ischemic Stroke: A Review. JAMA 325, 1088-1098

Mestre H, Hablitz LM, Xavier AL, Feng W, Zou W, Pu T, Monai H, Murlidharan G, Rivera RMC, Simon MJ (2018): Aquaporin-4-dependent glymphatic solute transport in the rodent brain. Elife 7, e40070

Mettimano M, Romano-Spica V, Ianni A, Specchia M, Migneco A, Savi L (2002): AGT and AT1R gene polymorphism in hypertensive heart disease. Int J Clin Pract 56, 574-577

Michels M, Sonai B, Dal-Pizzol F (2017): Polarization of microglia and its role in bacterial sepsis. J Neuroimmunol 303, 90-98

Mogensen FL, Delle C, Nedergaard M (2021): The Glymphatic System (En)during Inflammation. Int J Mol Sci 22

References

Mogoanta L, Ciurea M, Pirici I, Margaritescu C, Simionescu C, Ion DA, Pirici D (2014): Different dynamics of aquaporin 4 and glutamate transporter-1 distribution in the perineuronal and perivascular compartments during ischemic stroke. Brain Pathol 24, 475-493

Mosconi MG, Paciaroni M (2022): Treatments in Ischemic Stroke: Current and Future. Eur Neurol 85, 349-366

Nagaraja N, Tasneem N, Shaban A, Dandapat S, Ahmed U, Policeni B, Olalde H, Shim H, Samaniego EA, Pieper C, et al. (2018): Cerebral Microbleeds are an Independent Predictor of Hemorrhagic Transformation Following Intravenous Alteplase Administration in Acute Ischemic Stroke. J Stroke Cerebrovasc Dis 27, 1403-1411

Nayak AR, Kashyap RS, Kabra D, Purohit HJ, Taori GM, Daginawala HF (2012): Time course of inflammatory cytokines in acute ischemic stroke patients and their relation to inter-alfa trypsin inhibitor heavy chain 4 and outcome. Ann Indian Acad Neurol 15, 181-185

Ospel JM, Holodinsky JK, Goyal M (2020): Management of Acute Ischemic Stroke Due to Large-Vessel Occlusion: JACC Focus Seminar. J Am Coll Cardiol 75, 1832-1843

Pekny M, Pekna M (2014): Astrocyte reactivity and reactive astrogliosis: costs and benefits. Physiol Rev 94, 1077-1098

Pekny M, Wilhelmsson U, Pekna M (2014): The dual role of astrocyte activation and reactive gliosis. Neurosci Lett 565, 30-38

Peters PJ, Pierson J (2008): Immunogold labeling of thawed cryosections. Methods Cell Biol 88, 131-149

Pignataro G, Sirabella R, Anzilotti S, Di Renzo G, Annunziato L (2014): Does Na^+/Ca^{2+} exchanger, NCX, represent a new druggable target in stroke intervention? Transl Stroke Res 5, 145-155

Prabhakaran S, Ruff I, Bernstein RA (2015): Acute stroke intervention: a systematic review. JAMA 313, 1451-1462

Qin C, Zhou LQ, Ma XT, Hu ZW, Yang S, Chen M, Bosco DB, Wu LJ, Tian DS (2019): Dual Functions of Microglia in Ischemic Stroke. Neurosci Bull 35, 921-933

Radak D, Katsiki N, Resanovic I, Jovanovic A, Sudar-Milovanovic E, Zafirovic S, Mousad SA, Isenovic ER (2017): Apoptosis and Acute Brain Ischemia in Ischemic Stroke. Curr Vasc Pharmacol 15, 115-122

Ren Z, Iliff JJ, Yang L, Yang J, Chen X, Chen MJ, Giese RN, Wang B, Shi X, Nedergaard M (2013): 'Hit & Run' model of closed-skull traumatic brain injury (TBI) reveals complex patterns of post-traumatic AQP4 dysregulation. J Cereb Blood Flow Metab 33, 834-845

Rink C, Khanna S (2011): MicroRNA in ischemic stroke etiology and pathology. Physiol Genomics 43, 521-528

Samdani AF, Dawson TM, Dawson VL (1997): Nitric oxide synthase in models of focal ischemia. Stroke 28, 1283-1288

Shi K, Tian DC, Li ZG, Ducruet AF, Lawton MT, Shi FD (2019): Global brain inflammation in stroke. Lancet Neurol 18, 1058-1066

Shi Q, Cheng Q, Chen C (2021): The Role of Autophagy in the Pathogenesis of Ischemic Stroke. Curr Neuropharmacol 19, 629-640

Shi W-Z, Zhao C-Z, Zhao B, Shi Q-J, Zhang L-H, Wang Y-F, Fang S-H, Lu Y-B, Zhang W-P, Wei E-Q (2012): Aggravated inflammation and increased expression of cysteinyl leukotriene receptors in the brain after focal cerebral ischemia in AQP4-deficient mice. Neuroscience Bulletin 28, 680-692

Sieweke MH, Allen JE (2013): Beyond stem cells: self-renewal of differentiated macrophages. Science 342, 1242974

Smith AJ, Duan T, Verkman AS (2019): Aquaporin-4 reduces neuropathology in a mouse model of Alzheimer's disease by remodeling peri-plaque astrocyte structure. Acta Neuropathol Commun 7, 74

Sofroniew MV (2009): Molecular dissection of reactive astrogliosis and glial scar formation. Trends Neurosci 32, 638-647

Song Y, Li Z, He T, Qu M, Jiang L, Li W, Shi X, Pan J, Zhang L, Wang Y (2019): M2 microglia-derived exosomes protect the mouse brain from ischemia-reperfusion injury via exosomal miR-124. Theranostics 9, 2910

Song Y, Li Z, He T, Qu M, Jiang L, Li W, Shi X, Pan J, Zhang L, Wang Y, et al. (2019): M2 microglia-derived exosomes protect the mouse brain from ischemia-reperfusion injury via exosomal miR-124. Theranostics 9, 2910-2923

Stoll G, Jander S, Schroeter M (1998): Inflammation and glial responses in ischemic brain lesions. Prog Neurobiol 56, 149-171

Su Y, Fan W, Ma Z, Wen X, Wang W, Wu Q, Huang H (2014): Taurine improves functional and histological outcomes and reduces inflammation in traumatic brain injury. Neuroscience 266, 56-65

Suardika A, Astawa Pemayun TG (2018): New insights on the pathogenesis of endometriosis and novel non-surgical therapies. J Turk Ger Gynecol Assoc 19, 158-164

Sun C, Lin L, Yin L, Hao X, Tian J, Zhang X, Ren Y, Li C, Yang Y (2022): Acutely Inhibiting AQP4 With TGN-020 Improves Functional Outcome by Attenuating Edema and Peri-Infarct Astrogliosis After Cerebral Ischemia. Front Immunol 13, 870029

Sun H, Liang R, Yang B, Zhou Y, Liu M, Fang F, Ding J, Fan Y, Hu G (2016): Aquaporin-4 mediates communication between astrocyte and microglia: Implications of neuroinflammation in experimental Parkinson's disease. Neuroscience 317, 65-75

Tang Z, Yang G, Liao Z, Chen F, Chen S, Wang W, Huo G, Sun X, Wang X (2022): Tanshinone IIA reduces AQP4 expression and astrocyte swelling after OGD/R by inhibiting the HMGB1/RAGE/NF-κB/IL-6 pro-inflammatory axis. Sci Rep 12, 14110

Taussky P, Tawk RG, Daugherty WP, Hanel RA (2011): Medical therapy for ischemic stroke: review of intravenous and intra-arterial treatment options. World Neurosurg 76, S9-15

Théry C, Witwer KW, Aikawa E, Alcaraz MJ, Anderson JD, Andriantsitohaina R, Antoniou A, Arab T, Archer F, Atkin‐Smith GK (2018): Minimal information for studies of extracellular vesicles 2018 (MISEV2018): a position statement of the International Society for Extracellular Vesicles and update of the MISEV2014 guidelines. J Extracell Vesicles 7, 1535750

Thietart S, Rautou P-E (2020): Extracellular vesicles as biomarkers in liver diseases: a clinician's point of view. Journal of hepatology 73, 1507-1525

Tian Y, Zhu P, Liu S, Jin Z, Li D, Zhao H, Zhu X, Shu C, Yan D, Dong Z (2019): IL-4-polarized BV2 microglia cells promote angiogenesis by secreting exosomes. Adv Clin Exp Med 28, 421-430

Troili F, Cipollini V, Moci M, Morena E, Palotai M, Rinaldi V, Romano C, Ristori G, Giubilei F, Salvetti M, et al. (2020): Perivascular Unit: This Must Be the Place. The Anatomical Crossroad Between the Immune, Vascular and Nervous System. Front Neuroanat 14, 17

Trouillas P, von Kummer R (2006): Classification and pathogenesis of cerebral hemorrhages after thrombolysis in ischemic stroke. Stroke 37, 556-561

Turnbull MT, Zubair AC, Meschia JF, Freeman WD (2019): Mesenchymal stem cells for hemorrhagic stroke: status of preclinical and clinical research. NPJ Regen Med 4, 10

Unterberg A, Juettler E (2007): The role of surgery in ischemic stroke: decompressive surgery. Curr Opin Crit Care 13, 175-179

Uyeki TM, Mehta AK, Davey Jr RT, Liddell AM, Wolf T, Vetter P, Schmiedel S, Grünewald T, Jacobs M, Arribas JR (2016): Clinical management of Ebola virus disease in the United States and Europe. N Engl J Med 374, 636-646

Van Niel G, d'Angelo G, Raposo G (2018): Shedding light on the cell biology of extracellular vesicles. Nat Rev Mol Cell Biol 19, 213-228

Vu Q, Xie K, Eckert M, Zhao W, Cramer S (2014): Meta-analysis of preclinical studies of mesenchymal stromal cells for ischemic stroke. Neurology 82, 1277-1286

Wafa HA, Wolfe CDA, Emmett E, Roth GA, Johnson CO, Wang Y (2020): Burden of Stroke in Europe: Thirty-Year Projections of Incidence, Prevalence, Deaths, and Disability-Adjusted Life Years. Stroke 51, 2418-2427

Wang J, Xing H, Wan L, Jiang X, Wang C, Wu Y (2018): Treatment targets for M2 microglia polarization in ischemic stroke. Biomed Pharmacother 105, 518-525

Wang W, Huang XR, Li AG, Liu F, Li J-H, Truong LD, Wang XJ, Lan HY (2005): Signaling mechanism of TGF-β1 in prevention of renal inflammation: role of Smad7. J Am Soc Nephrol 16, 1371-1383

Wei H, Chen J, Wang S, Fu F, Zhu X, Wu C, Liu Z, Zhong G, Lin J (2019): A Nanodrug Consisting Of Doxorubicin And Exosome Derived From Mesenchymal Stem Cells For Osteosarcoma Treatment In Vitro. Int J Nanomedicine 14, 8603-8610

Wei W, Pan Y, Yang X, Chen Z, Heng Y, Yang B, Pu M, Zuo J, Lai Z, Tang Y, et al. (2022): The Emerging Role of the Interaction of Extracellular Vesicle and Autophagy-Novel Insights into Neurological Disorders. J Inflamm Res 15, 3395-3407

White HD, Simes RJ, Anderson NE, Hankey GJ, Watson JD, Hunt D, Colquhoun DM, Glasziou P, MacMahon S, Kirby AC, et al. (2000): Pravastatin therapy and the risk of stroke. N Engl J Med 343, 317-326

Wierońska JM, Cieślik P, Kalinowski L (2021): Nitric Oxide-Dependent Pathways as Critical Factors in the Consequences and Recovery after Brain Ischemic Hypoxia. Biomolecules 11

Xie L, Kang H, Xu Q, Chen MJ, Liao Y, Thiyagarajan M, O'Donnell J, Christensen DJ, Nicholson C, Iliff JJ (2013): Sleep drives metabolite clearance from the adult brain. Science 342, 373-377

Xin WQ, Wei W, Pan YL, Cui BL, Yang XY, Bähr M, Doeppner TR (2021): Modulating poststroke inflammatory mechanisms: Novel aspects of mesenchymal stem cells, extracellular vesicles and microglia. World J Stem Cells 13, 1030-1048

Xiong F, Liao X, Xiao J, Bai X, Huang J, Zhang B, Li F, Li P (2022): Emerging Limb Rehabilitation Therapy After Post-stroke Motor Recovery. Front Aging Neurosci 14, 863379

Xiong XY, Liu L, Yang QW (2016): Functions and mechanisms of microglia/macrophages in neuroinflammation and neurogenesis after stroke. Prog Neurobiol 142, 23-44

Xu S, Lu J, Shao A, Zhang JH, Zhang J (2020): Glial Cells: Role of the Immune Response in Ischemic Stroke. Front Immunol 11, 294

Yang D, Zhang W, Zhang H, Zhang F, Chen L, Ma L, Larcher LM, Chen S, Liu N, Zhao Q (2020): Progress, opportunity, and perspective on exosome isolation-efforts for efficient exosome-based theranostics. Theranostics 10, 3684

Yang H, Chen J (2022): Bone marrow mesenchymal stem cell-derived exosomes carrying long noncoding RNA ZFAS1 alleviate oxidative stress and inflammation in ischemic stroke by inhibiting microRNA-15a-5p. Metab Brain Dis 37, 2545-2557

Yang Q, Tong X, Schieb L, Vaughan A, Gillespie C, Wiltz JL, King SC, Odom E, Merritt R, Hong Y (2017): Vital signs: recent trends in stroke death rates—United States, 2000–2015. MMWR Morb Mortal Wkly Rep 66, 933

Yaswen L, Kulkarni AB, Fredrickson T, Mittleman B, Schiffman R, Payne S, Longenecker G, Mozes E, Karlsson S (1996): Autoimmune manifestations in the transforming growth factor-beta 1 knockout mouse. Blood 87, 1439-45.

Zamani P, Fereydouni N, Butler AE, Navashenaq JG, Sahebkar A (2019): The therapeutic and diagnostic role of exosomes in cardiovascular diseases. Trends Cardiovasc Med 29, 313-323

Zeppenfeld DM, Simon M, Haswell JD, D'Abreo D, Murchison C, Quinn JF, Grafe MR, Woltjer RL, Kaye J, Iliff JJ (2017): Association of perivascular localization of aquaporin-4 with cognition and Alzheimer disease in aging brains. JAMA Neurol 74, 91-99

References

Zhang D, Cai G, Liu K, Zhuang Z, Jia K, Pei S, Wang X, Wang H, Xu S, Cui C (2021): Microglia exosomal miRNA-137 attenuates ischemic brain injury through targeting Notch1. Aging (Albany NY) 13, 4079

Zhang F, Zhang JG, Yang W, Xu P, Xiao YL, Zhang HT (2018): 6-Gingerol attenuates LPS-induced neuroinflammation and cognitive impairment partially via suppressing astrocyte overactivation. Biomed Pharmacother 107, 1523-1529

Zhang L, Wei W, Ai X, Kilic E, Hermann DM, Venkataramani V, Bähr M, Doeppner TR (2021a): Extracellular vesicles from hypoxia-preconditioned microglia promote angiogenesis and repress apoptosis in stroke mice via the TGF-β/Smad2/3 pathway. Cell Death Dis 12, 1068

Zhang L, Graf I, Kuang Y, Zheng X, Haupt M, Majid A, Kilic E, Hermann DM, Psychogios MN, Weber MS, et al. (2021b): Neural Progenitor Cell-Derived Extracellular Vesicles Enhance Blood-Brain Barrier Integrity by NF-κB (Nuclear Factor-κB)-Dependent Regulation of ABCB1 (ATP-Binding Cassette Transporter B1) in Stroke Mice. Arterioscler Thromb Vasc Biol 41, 1127-1145

Zhang R, Wu Y, Xie F, Zhong Y, Wang Y, Xu M, Feng J, Charish J, Monnier PP, Qin X (2018): RGMa mediates reactive astrogliosis and glial scar formation through TGFβ1/Smad2/3 signaling after stroke. Cell Death Differ 25, 1503-1516

Zhang Y, Liu Y, Liu H, Tang WH (2019): Exosomes: biogenesis, biologic function and clinical potential. Cell Biosci 9, 1-18

Zhang Y, Chopp M, Meng Y, Katakowski M, Xin H, Mahmood A, Xiong Y (2015): Effect of exosomes derived from multipluripotent mesenchymal stromal cells on functional recovery and neurovascular plasticity in rats after traumatic brain injury. J Neurosurg 122, 856-867

Zhao Y, Zhang X, Chen X, Wei Y (2022): Neuronal injuries in cerebral infarction and ischemic stroke: From mechanisms to treatment (Review). Int J Mol Med 49

Zheng X, Haupt M, Bähr M, Tatenhorst L, Doeppner TR: Treating Cerebral Ischemia: Novel Therapeutic Strategies from Experimental Stroke Research. In: Pluta R (Hrsg): Cerebral Ischemia. Exon Publications

Zheng X, Zhang L, Kuang Y, Venkataramani V, Jin F, Hein K, Zafeiriou MP, Lenz C, Moebius W, Kilic E, et al. (2021b): Extracellular Vesicles Derived from Neural Progenitor Cells--a Preclinical Evaluation for Stroke Treatment in Mice. Transl Stroke Res 12, 185-203

Zheng Y, He R, Wang P, Shi Y, Zhao L, Liang J (2019): Exosomes from LPS-stimulated macrophages induce neuroprotection and functional improvement after ischemic stroke by modulating microglial polarization. Biomater Sci 7, 2037-2049

Zhong K, Wang RX, Qian XD, Yu P, Zhu XY, Zhang Q, Ye YL (2020): Neuroprotective effects of saffron on the late cerebral ischemia injury through inhibiting astrogliosis and glial scar formation in rats. Biomed Pharmacother 126, 110041

Zhu A, Lin Y, Hu X, Lin Z, Lin Y, Xie Q, Ni S, Cheng H, Lu Q, Lai S, et al. (2022): Treadmill exercise decreases cerebral edema in rats with local cerebral infarction by modulating AQP4 polar expression through the caveolin-1/TRPV4 signaling pathway. Brain Res Bull 188, 155-168

Zhu DD, Yang G, Huang YL, Zhang T, Sui A, Li N, Su WH, Sun HL, Gao JJ, Ntim M, et al. (2022): AQP4-A25Q Point Mutation in Mice Depolymerizes Orthogonal Arrays of Particles and Decreases Polarized Expression of AQP4 Protein in Astrocytic Endfeet at the Blood-Brain Barrier. J Neurosci 42, 8169-8183.

FUNDING RELATED TO THIS THESIS

The China Scholarship Council provided funding for this project's implementation [No. 202006940016].

ACKNOWLEDGEMENTS

I want to start by thanking Prof. Thorsten Roland Döppner, my supervisor, for letting me pursue a doctoral degree at University Medical Center Göttingen. Under the diligent direction and evaluation of my supervisor, I was able to finish the project's concept, carry out the experiment, and write the thesis. His serious scientific outlook, demanding scholastic spirit, and excellent work ethic had a profound influence on me and motivated me.

My profound gratitude goes out to Prof. Gerald Wulf, my second supervisor, for finishing the design of my experiment by submitting multiple progress reports.

I need to deliver my appreciation to Prof. Xinyu Yang and the China Scholarship Council for their outstanding assistance with my medical doctoral program application and doctoral studies. I would not be here without their attention.

I want to express my great appreciation to Dr. Lars Tatenhorst and Irina Graf from our research group who taught me experimental techniques and discussed project design. Whenever I encountered difficulties in the experiments, they were always there to give me the greatest help.

Additionally, I would like to thank all my teammates, including Wei Wei, Yongli Pan, Dr. Lin Zhang, Dr. Yaoyun Kuang, and Dr. Xuan Zheng, to help me with my study and life here.

I appreciate everything.

CURRICULUM VITAE

I am a male named Wenqiang Xin, and I was born on March 15, 1993, in Fuzhou, Jiangxi Province, China. Between August 2012 and June 2017, I completed my undergraduate studies at Zhengzhou University with a Clinical Medicine major. Furthermore, I finished my master's degree study at Tianjin Medical University with a major in surgery from August 2017 to June 2020. In November 2020, with the great aid of a 3-year scholarship from the Chinese government, I began a medical doctoral program in the Neurology department of the Georg-August-University of Göttingen.